4.1.7. Deoxyadenosine 5′-[ethyl *N*-(L-prolyl)phosphoroamidate] (dA-phosmidosine) (9b). Compound **8b** (118 mg, 0.15 mmol) was dissolved in THF (1.5 mL), and $Bu_4NF{\cdot}H_2O$ (152 mg, 0.58 mmol) was added. After being stirred at room temperature for 6 h, the mixture was diluted with $CHCl_3$. The $CHCl_3$ solution was washed three times with 5% $NaHCO_3$, dried over Na_2SO_4, filtered, and evaporated under reduced pressure. The residue was dissolved in a 1% solution of TFA in water–acetonitrile (1:1, v/v, 1.5 mL). After being stirred at room temperature for 15 min, the mixture was diluted with distilled water. The aqueous solution was washed three times with $CHCl_3$, evaporated under reduced pressure, and coevaporated with distilled water under reduced pressure. The residue was chromatographed on a column of C_{18} by using medium pressure chromatography with solvent system I. The fractions containing **9b** were collected and lyophilized. The residue was rechromatographed on a column of C18 with water–acetonitrile (90:10, v/v) followed by lyophilization from its aqueous solution to give **9b** as the free form (48 mg, 72%): ^{1}H NMR (270 MHz, D_2O) δ 1.09 (3H, 2t, $J_{POCH2CH3}$ = 6.9 Hz), 1.81–2.02 (3H, m), 2.25–2.38 (1H, m), 2.57–2.66 (1H, m, $J_{2'\text{-}Ha,2'\text{-}Hb}$ = 6.6 Hz), 2.77–2.88 (1H, m), 3.24–3.41 (2H, m), 3.73–3.84 (2H, m, J_{POCH} = 10.6 Hz), 4.07–4.16 (3H, m), 4.24–4.25 (1H, m), 4.69–4.74 (1H, m, $J_{3',2'\text{-}Hb}$ = 4.3 Hz), 6.37 (1H, dd, $J_{1',2'\text{-}Ha}$ = 6.3 Hz, $J_{1',2'\text{-}Hb}$ = 6.6 Hz), 8.09 (1H, s), 8.27 (1H, 2s); ^{13}C NMR (D_2O) δ 17.9, 18.0, 26.4, 32.4, 41.3, 41.4, 48.8, 64.7, 65.0, 65.4, 65.47, 65.50, 65.58, 67.56, 67.64, 67.7, 67.8, 73.4, 86.28, 86.34, 87.8, 87.88, 87.91, 120.9, 141.9, 150.79, 150.82, 154.9, 157.6, 178.5, 178.6; ^{31}P NMR (D_2O) δ 10.57; ESI-mass *m/z* calcd for $C_{17}H_{27}N_7O_6P$ 456.1761; observed [M + H] 456.1582.

4.1.8. 7,8-Dihydro-8-oxodeoxyadenosine 5′-[ethyl *N*-(L-prolyl)phosphoroamidate] (8-oxo-dA-phosmidosine) (9c). This compound was synthesized in 58% yield as the free form in a manner similar to that described for the synthesis of **9b**: ^{1}H NMR (270 MHz, D_2O) δ 1.10–1.16 (3H, 2t, $J_{POCH2CH3}$ = 6.9 Hz), 1.90–2.07 (3H, m), 2.30–2.40 (2H, m, 3″-Hb), 3.15–3.39 (3H, m), 3.81–3.95 (2H, m, J_{POCH} = 9.9 Hz), 4.11 (4H, m), 4.71 (1H, m, 3′-H), 6,21 (1H, t, $J_{1',2'\text{-}Ha} = J_{1',2'\text{-}Hb}$ = 6.6 Hz), 7.98 (1H, s); ^{13}C NMR ($CDCl_3$) δ 17.9, 18.0, 26.4, 32.4, 37.6, 48.8, 64.7, 65.1, 65.3, 65.4, 67.96, 67.98, 68.03, 68.1, 73.4, 73.5, 84.05, 84.12, 86.8, 87.0, 106.4, 148.8, 149.5, 153.3, 155.1, 178.7, 178.8; ^{31}P NMR ($CDCl_3$) δ 10.79, 10.87. ESI-mass *m/z* calcd for $C_{17}H_{27}N_7O_7P$ 472.1710; observed [M + H] 472.5253.

4.1.9. 6-*N*-Acetyl-7,8-dihydro-8-oxodeoxyadenosine 5′-[ethyl *N*-(L-prolyl)phosphoroamidate] (N^6-Ac-dA-phosmidosine) (9d). This compound was synthesized in 29% yield as the free form in a manner similar to that described for the synthesis of **9b**: ^{1}H NMR (270 MHz, D_2O) δ 1.13 (3H, t, $J_{POCH2CH3}$ = 6.9 Hz), 1.96–2.07 (3H, m), 2.27–2.32 (4H, m), 3.30–3.44 (2H, m), 3.83–3.93 (2H, m), 4.09–4.22 (4H, m), 4.65–4.69 (1H, m), 5.17–5.20 (1H, m), 5.95 (1H, d, $J_{1',2'}$ = 4.6 Hz), 8.40 (1H, s); ^{13}C NMR (D_2O) δ 17.9, 18.0, 32.4, 48.8, 64.7, 65.1, 65.4, 65.5, 67.6, 67.7, 72.3, 73.2, 73.3, 84.5, 84.7, 88.8, 113.5, 140.3, 152.8, 153.0, 154.8, 175.2, 178.6, 178.7. ^{31}P NMR (D_2O) δ 10.70; ESI-mass *m/z* calcd for $C_{19}H_{29}N_7O_9P$ 530.1764; observed [M + H] 530.1832.

4.1.10. Uridine 5′-[ethyl *N*-(L-prolyl)phosphoroamidate] (U-phosmidosine) (9e). This compound was synthesized in 91% yield as the free form in a manner similar to that described for the synthesis of **9b**: ^{1}H NMR (270 MHz, D_2O) δ 1.33–1.38 (3H, 2t, $J_{POCH2CH3}$ = 6.9 Hz), 2.01–2.18 (3H, m), 2.43–2.59 (1H, m), 3.34–3.51 (2H, m), 4.22–4.55 (8H, m, J_{POCH} = 11.2 Hz), 5.88–5.92 (2H, 2d, 1′-H, 5-H, $J_{1',2'}$ = 5.3 Hz), 7.74 (1H, 2d, $J_{6,5}$ = 8.2 Hz); ^{13}C NMR (D_2O) δ 18.1, 18.2, 26.4, 32.5, 48.9, 64.8, 65.2, 65.65, 65.68, 65.72, 67.17, 67.20, 67.22, 67.24, 67.27, 67.29, 67.3, 71.9, 70.0, 76.2, 76.3, 85.0, 85.1, 85.2, 85.3, 91.6, 104.8, 144.0, 144.1, 154.1, 168.6, 178.85, 178.88, 178.93, 179.0; ^{31}P NMR (D_2O) δ 11.07; ESI-mass *m/z* calcd for $C_{16}H_{26}N_4O_9P$ 449.1437; observed [M + H] 449.1453.

4.1.11. Cytidine 5′-[ethyl *N*-(L-prolyl)phosphoroamidate] (C-phosmidosine) TFA salt (9f). Compound **8f** (223 mg, 0.18 mmol) was dissolved in THF (1.8 mL), and $Bu_4NF{\cdot}H_2O$ (383 mg, 1.46 mmol) was added. After being stirred at room temperature for 1 h, the mixture was diluted with $CHCl_3$. The $CHCl_3$ solution was washed three times with 5% $NaHCO_3$, dried over Na_2SO_4, filtered, and evaporated under reduced pressure. The residue was dissolved in a 4% solution of TFA in water–acetonitrile (1:1, v/v, 1.8 mL). After the mixture was stirred at room temperature for 3 h, trifluoroacetic acid (73 μL, 0.99 mmol) was added. After being stirred at room temperature for an additional 12 h, the mixture was diluted with distilled water. The aqueous solution was washed 3 times with AcOEt, evaporated under reduced pressure, and coevaporated with distilled water under reduced pressure. The residue wad chromatographed on a column of C_{18} by using medium pressure chromatography with solvent system I. The fractions containing **9e** were collected and lyophilized. The residue was rechromatographed on a column of C_{18} with water–acetonitrile (95:5, v/v) followed by lyophilization from its aqueous solution to give **9f** as the TFA form (62 mg, 60%): ^{1}H NMR (270 MHz, D_2O) δ 1.32 (3H, t, $J_{POCH2CH3}$ = 6.9 Hz), 1.96–2.13 (3H, m), 2.47–2.52 (1H, m), 3.39–3.41 (2H, m), 4.18–4.49 (8H, m), 5.84–5.85 (1H, m), 6.11–6.13 (1H, m), 7.79–7.83 (1H, m); ^{13}C NMR (D_2O) δ 17.9, 18.01, 18.03, 26.1, 31.96, 31.99, 49.0, 49.2, 63.0, 63.2, 68.5, 68.56, 68.6, 69.1, 69.16, 69.23, 71.26, 71.33, 76.2, 84.0, 84.1, 93.1, 98.1, 112.3, 116.6, 120.9, 125.19, 145.1, 155.5, 155.6, 164.5, 165.0, 165.2, 165.3, 165.5, 166.1, 174.09, 174.12; ^{31}P NMR (D_2O) δ −0.90, −0.95; ESI-mass *m/z* calcd for $C_{16}H_{27}N_5O_8P$ 448.1597; observed [M + H] 448.1583.

4.1.12. Guanosine 5′-[ethyl *N*-(L-prolyl)phosphoroamidate] (G-phosmidosine) (9g). This compound was synthesized in 69% yield as the free form in a manner similar to that described for the synthesis of **9b**: ^{1}H NMR (270 MHz, D_2O) δ 1.16 (3H, t, $J_{POCH2CH3}$ = 7.3 Hz), 2.85–2.06 (3H, m), 2.26–2.39 (1H, m), 3.24–3.43 (2H, m), 3.81–3.97 (2H, m, J_{POCH} = 11.5 Hz), 4.09–4.32 (4H, m), 4.45–4.50 (1H, m), 4.68 (1H, m, $J_{2',3'}$ = 4.9 Hz), 5.83 (1H, d, $J_{1',2'}$ = 4.6 Hz), 7.92 (1H, d); ^{13}C NMR

(D_2O) δ 17.9, 17.95, 18.03, 18.1, 26.4, 32.4, 48.8, 64.7, 65.1, 65.5, 65.6, 65.7, 67.1, 67.2, 67.3, 67.4, 72.55, 72.59, 76.25, 76.30, 85.4, 85.5, 89.75, 89.78, 118.40, 118.43, 139.4, 139.5, 153.77, 153.80, 156.07, 156.09, 160.9, 178.6, 178.67, 178.70, 178.8; ^{31}P NMR (D_2O) δ 10.63, 10.73. ESI-mass *m/z* calcd for $C_{17}H_{27}N_7O_8P$ 488.1659; observed [M + H] 488.1658.

4.1.13. 7,8-Dihydro-8-oxodeoxyadenosine. 8-Bromodeoxyadenosine[21] (6.6 g, 20 mmol) was dissolved in a mixture of acetic acid–acetic anhydride (1:1, v/v, 400 mL), and sodium acetate (30 g, 366 mmol) was added. After being stirred at 120 °C for 30 min, the mixture was diluted with $CHCl_3$. The $CHCl_3$ solution was washed five times with distilled water, dried over Na_2SO_4, filtered, and evaporated under reduced pressure. The residue was dissolved in AcOEt. The AcOEt solution was washed 5% $NaHCO_3$, filtered, and evaporated under reduced pressure. The residue was dissolved in ethanol (86 mL), and NaOH (1.7 g, 43 mmol) was added. After being stirred at room temperature for 3 h, the mixture was stirred at 60 °C for an additional 1 h. The mixture was neutralized by addition of 4M HCl (10 mL) and 5% $NaHCO_3$. The precipitates were removed by filtration and washed three times with distilled water. The filtrate and washings were collected and evaporated under reduced pressure. The residue was chromatographed on a column of C_{18} with water–acetonitrile (100:0–98:2, v/v) to give the title compound as ocherous solids (1.6 g, 28%): ^{1}H NMR (270 MHz, DMSO-d_6) δ 1.92–2.00 (1H, m, $J_{2'\text{-Ha},2'\text{-Hb}}$ = 4.6 Hz), 2.89–2.99 (1H, m), 3.41–3.47 (1H, m), 3.57–3.63 (1H, m), 3.79–3.80 (1H, m), 4.36–4.38 (1H, m, $J_{3',2'\text{-Hb}}$ = 5.3 Hz), 6.13 (1H, dd, $J_{1',2'\text{-Ha}}$ = 6.3 Hz, $J_{1',2'\text{-Hb}}$ = 8.2 Hz), 7.19 (2H, br s), 7.91 (1H, s); ^{13}C NMR (DMSO-d_6) δ 36.5, 62.5, 71.5, 81.6, 87.5, 104.7, 146.1, 147.6, 149.7, 152.1. ESI-mass *m/z* calcd for $C_{10}H_{14}N_5O_4$ 268.1046; observed [M + H] 268.1027.

Acknowledgements

This work was supported by Grant-in-Aid for Scientific Research on Priority Areas (C) 'Genome Science' from the Ministry of Education, Culture, Sports, Science and Technology of Japan. This work was also supported by CREST of JST (Japan Science and Technology Corporation) and COE21 project.

References and notes

1. Uramoto, M.; Kim, C. J.; Shin-ya, K.; Kusakabe, H.; Isono, K.; Phillips, D. R.; McCloskey, J. A. *J. Antibiot.* **1991**, *44*, 375.
2. Phillips, D. R.; Uramoto, M.; Isono, K.; McCloskey, J. A. *J. Org. Chem.* **1993**, *58*, 854.
3. Matsuura, N.; Onose, R.; Osada, H. *J. Antibiot.* **1996**, *49*, 361.
4. Kakeya, H.; Onose, R.; Phillip, C.-C. L.; Onozawa, C.; Matsumura, F.; Osada, H. *Cancer Res.* **1998**, *58*, 704.
5. Moriguchi, T.; Asai, N.; Wada, T.; Seio, K.; Sasaki, T.; Sekine, M. *Tetrahedoron Lett.* **2000**, *41*, 5881.
6. Moriguchi, T.; Asai, N.; Okada, K.; Seio, K.; Sasaki, T.; Sekine, M. *J. Org. Chem.* **2002**, *67*, 3290.
7. Sekine, M.; Okada, K.; Seio, K.; Kakeya, H.; Osada, H.; Sasaki, T. *J. Org. Chem.* **2004**, *69*, 314.
8. Moriguchi, T.; Yanagi, T.; Wada, T.; Sekine, M. *Tetrahedron Lett.* **1998**, *39*, 3725.
9. Moriguchi, T.; Yanagi, T.; Kunimori, M.; Wada, T.; Sekine, M. *J. Org. Chem.* **2000**, *65*, 8229.
10. Filippov, D.; Timmers, C. M.; van der Marel, G. A.; van Boom, J. H. *Nucleos. Nucleot.* **1997**, *16*, 1403.
11. Filippov, D.; Timmers, C. M.; Roerdink, A. R.; van der Marel, G. A.; van Boom, J. H. *Tetrahedron Lett.* **1998**, *39*, 4891.
12. Jaeger, A.; Engels, J. *Tetrahedron Lett.* **1984**, *25*, 1437.
13. Ogilvie, K. K.; Beaucage, S. L.; Schifman, A. L.; Theriault, N. Y.; Sadana, K. L. *Can. J. Chem.* **1978**, *56*, 2768.
14. Zhang, W.; Robins, M. J. *Tetrahedron Lett.* **1992**, *33*, 1177.
15. Carmichael; DeGraff, W. G.; Gazar, A. F.; Minna, J. D.; Mitchell, J. B. *Cancer Res.* **1987**, *47*, 936.
16. Yu, X. Y.; Hill, J. M.; Yu, G.; Wang, W.; Kluge, A.; Wendler, P.; Gallant, P. *Bioorg. Med. Chem. Lett.* **1999**, *9*, 375–380, and references cited therein.
17. Heacock, D.; Forsyth, C. J.; Shiba, K.; Musier-Forsyth, K. *Bioorg. Chem.* **1996**, *24*, 273.
18. Castro-Pichel, J.; Garcia-Lopez, M. T.; de Las Heras, F. G. *Tetrahedron* **1987**, *43*, 383.
19. Isono, K.; Uramoto, M.; Kusakabe, H.; Miyata, N.; Koyama, T.; Ubukata, M.; Sethi, S. K.; McCloskey, J. A. *J. Antibiot.* **1984**, *37*, 670.
20. Davison, E. C.; Johnsson, K. *Nucleos. Nucleot.* **1993**, *12*, 237.
21. Catalanotti, B.; Galeone, A.; Gomez-Paloma, L.; Mayol, L.; Pepe, A. *Bioorg. Med. Chem. Lett.* **2000**, *10*, 2005.

Available online at www.sciencedirect.com
SCIENCE DIRECT
Tetrahedron
Tetrahedron 60 (2004) 7085–7091

RK-805, an endothelial-cell-growth inhibitor produced by *Neosartorya* sp., and a docking model with methionine aminopeptidase-2

Yukihiro Asami,[a,b] Hideaki Kakeya,[a,*] Rie Onose,[a] Yie-Hwa Chang,[c] Masakazu Toi[d] and Hiroyuki Osada[a,b,*]

[a]*Antibiotics Laboratory, Discovery Research Institute, RIKEN, 2-1 Hirosawa, Wako, Saitama 351-0198, Japan*
[b]*Graduate School of Science and Engineering, Saitama University, 255 Shimo-Okubo, Saitama, Saitama 338-8570, Japan*
[c]*Health Sciences Center, St. Louis University School of Medicine, 1402 S. Grand Blvd., St. Louis, MO 63104, USA*
[d]*Tokyo Metropolitan Komagome Hospital, 3-18-22 Honkomagome, Bunkyo-ku, Tokyo 113-8677, Japan*

Received 19 June 2003; revised 5 September 2003; accepted 5 September 2003

Available online 19 June 2004

Abstract—We found that a fungus *Neosartorya* sp. produced an angiogenesis inhibitor, RK-805. By spectroscopic analyses and semi-synthetic methods from fumagillin, the structure of RK-805 was identified as 6-oxo-6-deoxyfumagillol, which has not been reported as a natural product. RK-805 preferentially inhibited the growth of human umbilical vein endothelial cells (HUVECs) rather than that of human normal fibroblast in cell proliferation assays and blocked endothelial cell migration induced by vascular endothelial growth factor (VEGF). Moreover, RK-805 selectively inhibited methionine aminopeptidase-2 (MetAP2), but not methionine aminopeptidase-1 (MetAP1). The docked structure of RK-805 complexed with human MetAP2 indicated that not only a covalent bond between a nucleophilic imidazole nitrogen atom of His231 and the carbon of the reactive spirocyclic epoxide of RK-805, but also a hydrogen bond between NH (Asn329) and the carbonyl group of RK-805 at C-6 promote close contact in the binding pocket of the enzyme. Taken together, these results suggest that structure activity relationships of RK-805 derivatives at both C-4 and C-6, in comparison with ovalicin and TNP-470, would be useful for development of new angiogenesis inhibitors.

1. Introduction

Angiogenesis, the formation and growth of new blood capillaries from pre-existing vessels, is a vital function for the growth of normal tissues during embryogenesis, as well as for the malignant growth of solid tumors. The process of angiogenesis in endothelial cells consists of several distinct and sequential steps such as degradation of the basement membrane by proteolytic enzymes, migration (chemotaxis) toward the stimulus, proliferation, formation of vascular loops, maturation of neovessels, and neosynthesis of basement membrane constituents. Under pathological conditions, such as tumor progression, diabetic retinopathy, and rheumatoid arthritis, the control mechanisms can be disordered primarily by a number of angiogenic factors, and this process can lead to abnormal angiogenesis. The inhibition of angiogenesis is therefore emerging as a promising strategy to cure angiogenesis-related diseases.[1–4]

In this regard, several angiogenesis inhibitors derived both from natural products and by chemical synthesis have been studied. These include peptide inhibitors angiostatin,[5] endostatin,[6] and NK4,[7] as well as thalidomide,[8] TNP-470,[9] marimastat,[10] and SU6668,[11] which are small molecules. We have also established cell-based screening systems for identifying novel angiogenesis inhibitors blocking signaling pathway induced by vascular endothelial growth factor (VEGF) or exhibiting selective growth inhibitory activity in endothelial cells. Recently, we reported the identification of novel angiogenesis inhibitors, i.e. the highly functionalized pentaketide dimers epoxyquinols A and B,[12–15] and azaspirene[16,17] with a 1-oxa-7-azaspiro[4.4]non-2-ene-4,6-dione skeleton from fungal metabolites (Fig. 1).

In the course of our research to discover angiogenesis inhibitors among the secondary metabolites of microorganisms, RK-805 was discovered from the fermentation broth of a fungus, *Neosartorya* sp. The structure was elucidated as 6-oxo-6-deoxyfumagillol by spectroscopic analyses and chemical modifications of fumagillin. It is noted that RK-805 might be a precursor metabolite or be a shunt

Keywords: Angiogenesis inhibitor; Microbial metabolites; Endothelial cells; Methionine aminopeptidase-2; docking model.
* Corresponding authors. Tel.: +81-48-467-9542; fax: +81-48-462-4669; e-mail address: hkakeya@riken.jp

0040–4020/$ - see front matter © 2004 Elsevier Ltd. All rights reserved.
doi:10.1016/j.tet.2003.09.104

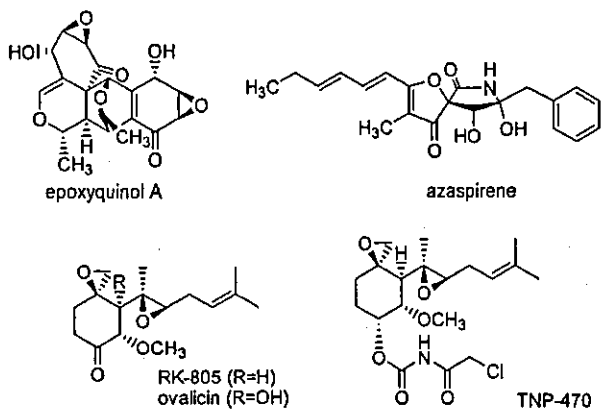

Figure 1. Structures of epoxyquinol A, azaspirene, RK-805, ovalicin, and TNP-470.

metabolite in fumagillin-biosynthesis. We describe in this paper the fermentation, isolation, structure elucidation, and the specificity and effects of RK-805 toward methionine aminopeptidase-2 (MetAP2) as well as growth and migration of endothelial cells.

2. Results and discussion

The producing strain, *Neosartorya* sp. was cultured in the fermantation medium (15 l) at 28 °C for 3 days, and the ethyl acetate extract of the whole broth was obtained. Then, the successive purification procedures by a silica gel column chromatography, a preparative reverse-phase HPLC, and a preparative TLC afforded 5.0 mg of RK-805 as a colorless oil. The molecular formula of RK-805 was determined to be $C_{16}H_{24}O_4$, based on the HREI-MS data (*m/z*: 280.1723); this formula was supported by ^1H and ^{13}C NMR spectrum data. The UV spectrum had an end absorption and an absorption maximum of the IR spectrum at 1730 cm^{-1} suggested the presence of a carbonyl group.

All single-bond connections between ^1H and ^{13}C in RK-805 were elucidated by PFG-HMQC and DEPT experiments. The NMR data and the molecular formula indicated the presence of one methoxy, three methyls, four methylenes, three sp^3 methines and one sp^2 methine, and four quaternary carbons, including a carbonyl carbon. As regards the $^1H-^1H$ correlations in PFG-DQFCOSY, H-11 through H-13 indicated the presence of olefinic protons and an epoxide methine (Fig. 2(A)). In addition, long range couplings from H-11 and H-15 to C-10 and from H-16 and H-17 to C-13 and C-14 were observed in an HMBC experiment (Fig. 2(A)). The cyclohexanone skeleton was confirmed by $^1H-^1H$ correlations on PFG-DQFCOSY: from H-4 to H-5 and H_2-7 to H_2-8, as well as by $^1H-^{13}C$ correlations in the PFG-HMBC spectra: the strong two-and three-bond $^1H-^{13}C$ correlations from H-4 and H-8 to C-3, from H-18 of the methoxy proton signal to C-5, and the correlations of the carbonyl carbon at C-6 with the protons on C-4, C-5, C-7, and C-8. The exocyclic epoxide ring on cyclohexanone was confirmed by the chemical shifts, coupling constants, and two-bond correlations from H-2 to C-3 in the PFG-HMBC spectrum. The relative configuration of RK-805 was elucidated by NOE experiments. Significant NOEs between

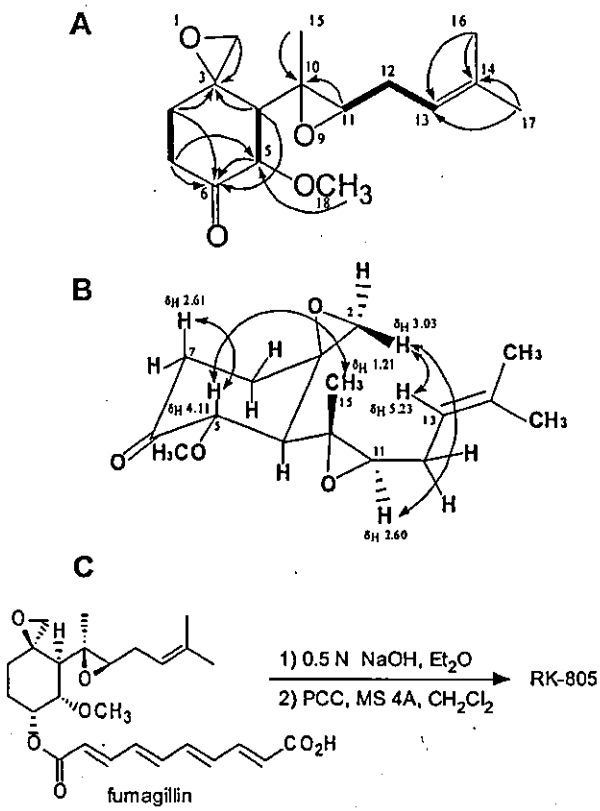

Figure 2. Structure determination of RK-805. (A) Key correlations in PFG-DQFCOSY and PFG-HMBC spectra in RK-805. The bold lines show the proton spin networks, and the arrows show the $^1H-^{13}C$ long-range correlations. (B) Summary of the NOE spectra. The arrows point to significant NOEs.

H-15 (δ_H 1.21) and H-5 (δ_H 4.11), H-13 (δ_H 5.23) and H-2 (δ_H 3.03), and H-11 (δ_H 2.60) and H-2 (δ_H 3.03) indicated a *trans* configuration for the epoxide on the side chain at C-4. The experimental results showed that no NOE was observed between H-15 (δ_H 1.21) and H-11 (δ_H 2.60), thereby also supporting this configuration. The NOE between H-5 (δ_H 4.11) and H-7 (δ_H 2.61) indicated a diaxial conformation for these protons (Fig. 2(B)). Moreover, the deduced structure was confirmed by chemical modifications from fumagillin: Hydolysis of fumagillin in the alkali condition, followed by oxidation with PCC to give synthetic RK-805 in 82% yield over two steps (Fig. 2(C)). The physico-chemical properties of natural RK-805 were identical with those of synthetic RK-805. Thus, the structure of RK-805 including its absolute configuration was determined to be 6-oxo-6-deoxyfumagillol, which has reported as a synthetic analogue of fumagillin and ovalicin.[18,19] The ^1H and ^{13}C NMR assignments for RK-805 are summarized in Section 4. It is possible that RK-805 is a precursor metabolite or is a shunt metabolite in fumagillin-biosynthesis, as fumagillin possesses a long aliphatic side chain at C-6 via an ester bond.

The core structure of RK-805 was similar to that of fumagillin and other fumagillin analogues, e.g. ovalicin[20] isolated from marine fungal metabolites and its synthetic analogue TNP-470 (*O*-(chloroacetylcarbamoyl)fumagillol, AGM-1470).[21] The structure of RK-805 is different from the structure of ovalicin and TNP-470 as regards the C-4 and

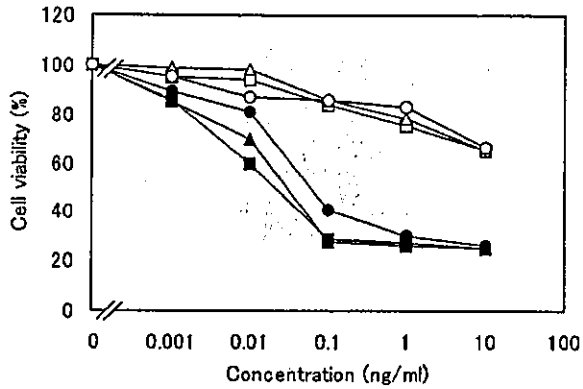

Figure 3. RK-805 effectively inhibits the growth of HUVECs. The growth of HUVECs: ■, Ovalicin (IC_{50}=0.02 ng/ml); ▲, RK-805 (IC_{50}=0.03 ng/ml); ●, TNP-470 (IC_{50}=0.06 ng/ml). The growth of WI-38 cells: □, Ovalicin ($IC_{50}\geq$10 ng/ml); △, RK-805 ($IC_{50}\geq$10 ng/ml); ○, TNP-470 ($IC_{50}\geq$10 ng/ml).

C-6 positions, respectively. Although the growth inhibitory activity by fumagillin-related compounds against human endothelial cells has been reported, little is known about their effects on the growth of human normal fibroblast. We therefore tested the inhibitory activity of RK-805 in both human umbilical vein endothelial cells (HUVECs) and normal human lung fibroblast WI-38 cells. RK-805, ovalicin, and TNP-470 did not exhibit remarkable inhibitory activity, even at 10 ng/ml, in WI-38 cells, whereas they did inhibit the cell growth of HUVECs in a dose-dependent manner, as shown in Figure 3. The IC_{50} values of RK-805, ovalicin, and TNP-470 were 0.03, 0.02, and 0.06 ng/ml, respectively, indicating that RK-805 exhibited selective inhibitory activity in HUVECs, as did both ovalicin and TNP-470.

We performed a chemotaxicell chamber assay, as there has been no report on the effect of RK-805 on endothelial cell migration in three-dimensional-cultutres systems of HUVECs. In this assay, HUVECs in the top chamber migrated and penetrated the filters, entering the lower chamber supplemented with 12.5 ng/ml of an angiogenic factor, VEGF-containing medium, as determined by counting the number of cells attached to the lower side of the filter after 18 h of incubation. VEGF significantly induced cell migration, whereas 10 μM of SU5614, an inhibitor of VEGF receptor tyrosine kinase,[22] inhibited the VEGF-induced cell migration. RK-805 also inhibited the cell migration induced by VEGF in a dose-dependent manner, without showing significant cell toxicity; this results was estimated by a trypan blue dye exclusion assay. The ED_{50} value of RK-805 was ca. 10 ng/ml, as shown in Figure 4. Ovalicin and TNP-470 exhibited almost the same inhibitory activity in this assay. These results suggest that RK-805 blocks the function of endothelial cell migration activated by VEGF.

Methionine aminopeptidase-2 (MetAP2) has been identified as the molecular target for the fumagillin family.[23–25] However, the selectivity of RK-805 against MetAP2 has been unclear. We therefore investigated the selective inhibitory effect of RK-805 on MetAP2 activity on agar plates containing the *map1* null strain, *Saccharomyces cerevisiae* (*MAP1/map1::HIS3*). The map1 null strain and the map2 null strain (*MAP2/map2::URA3*) is viable with a slower growth rate, whereas the *map1* and *map2* double-null strain is nonviable.[26] Although wild-type and *map2* null mutant are resistant to RK-805, ovalicin, and TNP-470, the growth of the *map1* null mutant was completely inhibited by these three fumagillin-related molecules (Fig. 5(A)–(C)). The inhibitory activities of RK-805 and ovalicin on MetAP2 were more potent than that of TNP-470 (Fig. 5(D)). These results indicate that yeast MetAP2, but not MetAP1, is a common target for RK-805, ovalicin, and TNP-470.

MetAPs, cobalt-containing metalloproteases, which remove the NH_2-terminal methionine from proteins in a non-processive manner, are highly conserved in *Escherichia coli*, *Saccharomyces cerevisiae*, and humans.[27–29] In 1998, Clardy, J. et al. revealed a covalent bond between an epoxide group on the cyclohexane ring of fumagillin and a histidine residue (His-231) at the active site of the human

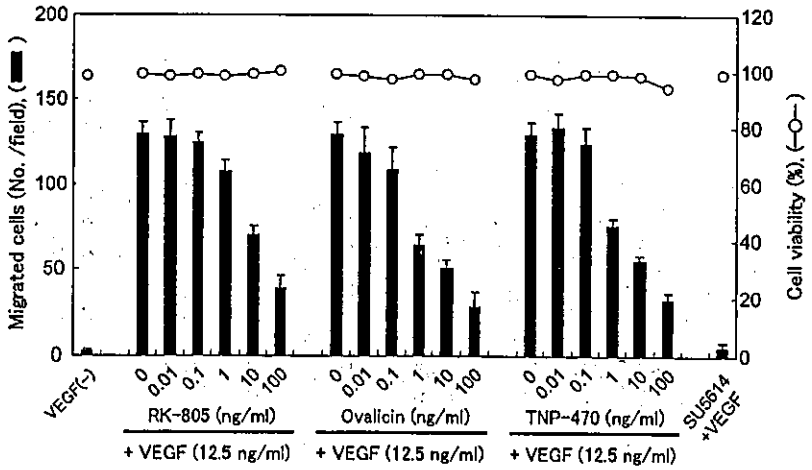

Figure 4. RK-805 blocks endothelial cell migration induced by VEGF. HUVECs stimulated upon VEGF-treatment were incubated with either various concentrations of RK-805, ovalicin, TNP-470, or 10 μM of SU5614 in the upper chamber for 18 h. Thereafter, the cells were fixed with MeOH and stained with Wright solution. The cells migrated to the lower surface, induced by VEGF, were counted manually under a microscope at a magnification of x100 (bold column). Values are the means±SD for triplicate samples. Cell viability was assessed by a trypan blue dye exclusion assay (bold line).

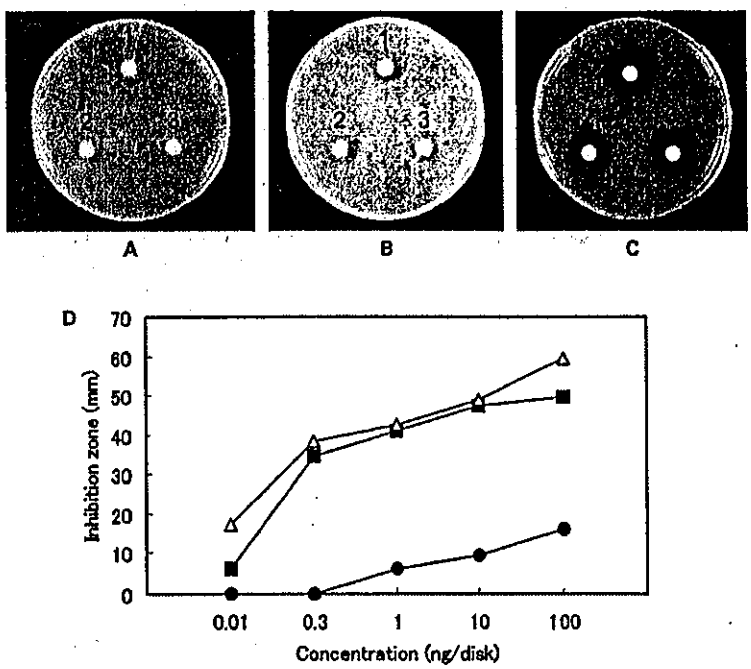

Figure 5. Selective MetAP2 inhibitory activity of RK-805. (A–C) Wild-type *Saccharomyces cerevisiae* W303 (A). *map2* null strain (*MAP2/map2::URA3*) (B). *map1* null strain (*MAP1/map1::HIS3*) (C). RK-805 (1, 0.3 ng/disk), Ovalicin (2, 0.3 ng/disk), and TNP-470 (3, 30 ng/disk). (D) Determination of respective MetAP2 inhibitory activities of the compounds using agar diffusion assays on the MetAP1 null strain (MAP1/map1::HIS3). Δ: RK-805, ■: ovalicin, ●: TNP-470.

MetAP2 crystal structure.[30] We investigated a three-dimensional model of human MetAP2 and RK-805 built from the known X-ray coordinates (PDB ID: 1B59) using a COMTEC 4D OCTANE 2, R12000A Workstation and Insight II. The predicted overall structure of RK-805 complexed with human MetAP2 is shown in Figure 6. The docked structure indicated that not only a covalent bond between an imidazole nitrogen atom of His231 and a carbon of the spirocyclic epoxide of RK-805, but also a hydrogen bond between NH (Asn329) and a carbonyl group of RK-805 promoted close contact to fit well in the binding pocket of the enzyme, even though RK-805 lacks the aliphatic side chain at C-6 of fumagillin and a hydroxyl group at the C-4 of ovalicin.

The development of angiogenesis inhibitors as novel anticancer agents has been one of the most challenging objectives of contemporary cancer research. Among several angiogenesis inhibitors characterized within the last decade, TNP-470, a synthetic analogue of fumagillin, is currently in clinical trials for the treatment of a variety of cancers, including solid tumors as well as Kaposi's sarcoma.[31,32] The fumagillin family has been shown to block endothelial cell proliferation and cell cycle progression of cells in the G1

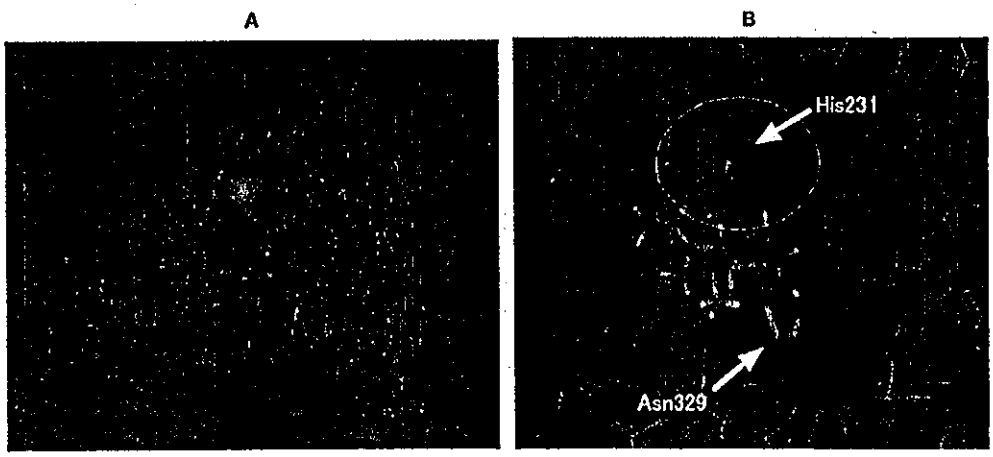

Figure 6. Proposed binding image of RK-805 complexed with human MetAP2. (A) Overall structure of the complex between MetAP-2 (PDB ID: 1B59) and RK-805. In the stick model, red indicates the atoms of RK-805 molecules in the active site. (B) A covalent bond is shown between an imidazole nitrogen atom of His231 and the carbon of the spirocyclic epoxide (yellow ring). The hydrogen bond between NH (Asn329) and the carbonyl group of RK-805 is shown (red ring). Carbon atoms are green, oxygen atoms are red, hydrogen atoms are white, and nitrogen atoms are blue.

phase.[9,33,34] Although MetAP2 has been identified as a molecular target of these compounds, it remains unclear how inhibition of this enzyme leads to cell cycle arrest, antiangiogenic activity, and in vivo antitumor effects. There could be a vital MetAP2-specific intracellular substrate that is sensitive to fumagillin-type drugs including RK-805. Turk, B. E. et al. reported that the in vitro inhibitory activity of RK-805 against MetAP2 activity was 15-fold and 6-fold less than that of ovalicin and TNP-470, respectively.[19] However, the potency of RK-805 and ovalicin in the endothelial assays (Figs. 3 and 4) and the yeast growth inhibition assay (Fig. 5) here is almost the same, suggesting that those compounds have different rates of cellular uptake and metabolism in intact cells. In addition, preliminary pharmacokinetic and metabolic experiments have indicated that TNP-470 was biotransformed in the primary cultures of human hepatocytes and in the microsomal fractions of various human tissues.[35] These finding have increased the hope of identifying a more stable analogue of fumagillin-type molecules. Therefore, structure activity relationships of analogues of RK-805 at both C-4 and C-6 would be useful for development of new MetAP2 inhibitors. Moreover, the potential therapeutic value of angiogenesis inhibitors has also been evaluated in combination with different anticancer modalities including chemotherapeutic agents, cytokines, and radiotherapy.[36] Thus, the identification of novel angiogenesis inhibitors would provide a range of tools that would be therapeutic in cases involving pathologic angiogenesis.

3. Conclusion

In conclusion, we identified RK-805, 6-oxo-6-deoxyfumagillol, as an angiogenesis inhibitor isolated from a fungus, *Neosartorya* sp., in an endothelial cell-based assay. RK-805 exhibited potent inhibitory activity not only as regards in endothelial cell growth, but also in VEGF-induced endothelial cell migration. In addition, RK-805 selectively inhibited MetAP2 activity, but not MetAP1 activity. The important aspect of the binding model of RK-805 with human MetAP2 was that a carbonyl group of RK-805 formed a hydrogen bond with NH (Asn329) at the active site of the enzyme, which was not seen in the case of fumagillin or TNP-470. RK-805 is a promising agent in this context; a structure-based drug design that would include a modification of this carbonyl group might shed light on the development of novel angiogenesis inhibitors. Further study of structure-activity relationships and novel bioactive natural products is currently underway.

4. Experimental

4.1. General

Optical rotation was recorded on a JASCO DIP-370 spectrometer and the IR spectra were obtained on a SHIMADZU FT-IR 8100M spectrophotometer. ^{1}H and ^{13}C NMR spectra were taken on a JEOL ECP-500 NMR spectrometer. The mass spectra were measured on a JEOL JMS-SX102. Chemical shifts are reported in parts per million relative to acetone (^{1}H, δ 2.04; ^{13}C, δ 29.8). Data for ^{1}H NMR are reported as follows: chemical shift, assignment, integration, multiplicity (s=singlet, d=doublet, t=triplet, q=quartet, m=multiplet), and coupling constants. Data for ^{13}C NMR are reported as follows: chemical shift, assignment, and multiplicity (s=singlet, d=doublet, t=triplet, q=quartet).

4.2. Fermentation and purification

The producing strain *Neosartorya* sp. was inoculated into two 500 ml Erlenmeyer flasks containing 75 ml of a sterile seed medium and was incubated on a rotary shaker at 28 °C for 3 days. The seed medium was composed of soluble starch 2%, glucose 1%, soybean meal 1.5%, malt extract 0.5%, potato dextrose 10%, vegetable extract 10%, $MgSO_4 \cdot 7H_2O$ 0.05%, and KH_2PO_4 0.05%. This seed medium (150 ml) was transferred to 15 l of the same production medium in a 30-L jar fermentor. The fermentation was carried out at 28 °C for 3 days with agitation at 350 rpm and an air flow of 15 l min^{-1}. The culture broth was centrifuged and the mycelial cake was extracted with acetone. The extract was concentrated in vacuo to an aqueous solution, which was extracted with an equal volume of ethyl acetate. The organic layer was concentrated in vacuo to dryness. The concentrate was applied to silica gel column chromatography. The materials were eluted with a stepwise gradient of $CHCl_3$–CH_3OH. The active fraction in $CHCl_3$–CH_3OH (50:1) was concentrated in vacuo to yield an oily material. Further purification of RK-805 was carried out by reverse-phase HPLC using a preparative ODS column (2 i.d.×25 cm, Senshu Scientific Co. Ltd., Tokyo, Japan). Finally, 5.0 mg of RK-805 was purified by preparative TLC with $CHCl_3$–CH_3OH (50:1).

4.3. Physico-chemical properties of RK-805

Colorless oil; HREI-MS *m/z*: 280.1723 (calcd for $C_{16}H_{24}O_4$: 280.1675); UV λ_{max} (MeOH) nm: End abs.; IR ν_{max} (neat) cm^{-1}: 2950, 1730, 1650, 1120; $[\alpha]_D^{20}=-61.3°$ (*c* 0.30, $CHCl_3$), lit.[18] $[\alpha]_D^{24}=-64.9°$ (*c* 0.21, $CHCl_3$); the R_f value in the solvent system of $CHCl_3$–MeOH (50:1) was 0.46 on a silica gel TLC (Merck 60 F_{254}). The *Rt* was 17.1 min in HPLC analysis: PEGASIL ODS (4.6 i.d. ×250 mm, Senshu Scientific Co. Ltd., Tokyo, Japan); flow rate, 1 ml/min; detection, 215 nm; mobile phase, a linear gradient solvent system CH_3CN–H_2O from 20:80 to 100:0 for 20 min. ^{1}H NMR (500 MHz, acetone-d_6) δ 1.21 (15-H, 3H, s), 1.64 (16-H, 3H, s), 1.66 (8-H_a, 1H, ddd, *J*=3.5, 5.3, 13.0 Hz), 1.72 (17-H, 3H, s), 1.88 (4-H, 1H, d, *J*=10.6 Hz), 2.08 (8-H_b, 1H, ddd, *J*=1.3, 5.3, 13.0 Hz), 2.23 (12-H, 2H, m), 2.36 (7-H_a, 1H, ddd, *J*=1.3, 5.3, 14.2 Hz), 2.60 (11-H, 1H, t, *J*=6.3 Hz), 2.61 (7-Hb, 1H, m), 2.72 (2-Ha, 1H, d, *J*=4.6 Hz), 3.03 (2-H_b, 1H, d, *J*=4.6 Hz), 3.38 (18-H, 3H, s), 4.11 (5-H, 1H, d, *J*=10.6 Hz), 5.23 (13-H, 1H, t, *J*=7.4 Hz); ^{13}C NMR (125 MHz, acetone-d_6) δ 14.35 (15-C, q), 17.98 (16-C, q), 25.80 (C-17, q), 28.14 (C-12, t), 33.58 (C-8, t), 37.39 (C-7, t), 52.35 (C-2, t), 53.89 (C-4, d), 57.89 (C-18, q), 59.19 (C-10, s), 59.29 (C-3, s), 60.60 (C-11, d), 83.84 (C-5, d), 120.10 (C-13, d), 134.79 (C-14, s), 207.28 (C-6, s).

4.4. Synthesis of RK-805

Fumagillin (0.9 mg, 0.0020 mmol) was added to a 0.5 N

$NaOH-Et_2O$ solution (1 ml, v/v=1:1), and was stirred at room temperature for 2.5 h. Then, the reaction mixture was diluted with H_2O and Et_2O, and extracted with Et_2O. The resulting organic layer was washed with brine, dried over Na_2SO_4, and concentrated in vacuo to afford 0.54 mg (quant.) of fumagillol. To a suspension of PCC (1 mg, 0.0046 mmol) and powdered molecular sieves 4A (3.0 mg) in CH_2Cl_2 (1 ml) was added a solution of the above fumagillol solution in CH_2Cl_2 (0.5 ml) stirring in an ice-water bath. The mixture was stirred for 1 h at room temperature. Florisil and CH_2Cl_2 were added to the mixture, which was filtered through a pad of Celite and Florisil, and the filtrate was concentrated in vacuo. The residue was purified by preparative TLC with $CHCl_3-CH_3OH$ (50:1) to give synthetic RK-805 (0.45 mg, 82.0% yield in two steps).

4.5. Endothelial cell proliferation assay

Human umbilical vein endothelial cells (HUVECs) were cultured in Humedia-EG2 medium (KURABO, Osaka, Japan) at 37 °C under a 5% CO_2 atmosphere. WI-38 cells (normal human lung fibroblast cells) were cultured in DMEM (Dulbecco's modified eagle medium) containing 10% fetal calf serum in a 5% CO_2 incubator at 37 °C. Sub-confluently growing (80%-90%) cells were trypsinized. HUVECs and WI-38 cells were seeded on 96-well microplates ($1.5-3.0\times10^3$ cells per well). Test compounds were added, and further incubated for 48 h (WI-38 cells) or 96 h (HUVECs). The cell number was evaluated by the subsequent color reaction. 2-(2-methoxy-4-nitrophenyl)-3-(4-nitrophenyl)-5-(2,4-disulfophenyl)-2*H*-tetrazolium, monosodium salt, WST-8™ (Nacalai Tesque, Kyoto, Japan) was added, and the cells were further incubated for 3–4 h at 37 °C. The absorbance (A_{450}) of each well was measured by a Wallac 1420 multilabel counter (Amersham Biosciences, Piscataway, NJ). Each result is the mean±S.D. (n=three experiments).

4.6. Endothelial cell migration assay

Human umbilical vein endothelial cells (HUVECs) (1×10^5 cells) suspended in Humedia-EG2 medium with various concentrations of test compounds were added to the upper compartment of a chemotaxicell chamber (KURABO, Osaka) and incubated with HuMedia-EG2 medium containing 12.5 ng/ml of VEGF in the lower compartment for 18 h at 37 °C in a 5% CO_2 atmosphere. The filter was fixed with MeOH and stained with Wright solution. The cells on the upper surface of the filter were removed by wiping the filter with cotton swabs. Cells that migrated through the filter to the lower surface were counted manually under a microscope at a magnification of ×100. Values are means±SD for triplicate samples. Cell viability was assessed by a trypan blue dye exclusion assay.

4.7. Yeast growth inhibition assay

Inhibition of MetAP2 activity was determined on an agar plate containing the *map1* null strain (*MAP1/map1::HIS3*), *Saccahromyces cerevisiae*.[25] Sterile filter disks impregnated with 10 μl of compounds were placed on the assay plate, and the plates were further incubated at 30 °C for 72 h. As references, wild-type strain *S. cerevisiae* W303 and the *map2* null strain (*MAP2/map2::URA3*) were also tested.[25]

4.8. Molecular modeling of RK-805 on MetAP2

The computer model of the binding image was constructed by means of a COMTEC 4D OCTANE 2, R12000A Workstation (Silicon Graphics, Inc., Mountain View, CA) and Insight II (Accelrys, Inc., San Diego, CA).

Acknowledgements

This work was supported in part by a Special Project Funding for Basic Science (Chemical Biology Research) from RIKEN, and a grant from the Ministry of Education, Culture, Sports, Science and Technology, Japan. We are grateful to Ishida, K. (RIKEN) for his valuable suggestions concerning the docking model.

References and notes

1. Kerbel, R.; Folkman, J. *Nat. Rev. Cancer* **2002**, *2*, 727–739.
2. Cristofanilli, M.; Charnsangavej, C.; Hortobagyi, G. N. *Nat. Rev. Drug Disc.* **2002**, *1*, 415–425.
3. Gasparini, G. *Drugs* **1998**, *58*, 17–38.
4. Shibuya, M. *Cell Struct. Funct.* **2001**, *26*, 25–35.
5. O'Reilly, M. S.; Holmgren, L.; Shing, U.; Chen, C.; Rosenthal, R. A.; Moses, M.; Lane, W. S.; Cao, Y.; Sage, E. H.; Folkman, J. *Cell* **1994**, *79*, 315–328.
6. O'Reilly, M. S.; Boehm, T.; Shing, Y.; Fukai, N.; Vasios, G.; Lane, W. S.; Flynn, E.; Birkhead, J. R.; Olsen, B. R.; Folkman, J. *Cell* **1997**, *88*, 277–285.
7. Nakabayashi, M.; Morishita, R.; Nakagami, H.; Kuba, K.; Matsumoto, K.; Nakamura, T.; Tano, Y.; Kaneda, Y. *Diabetologia* **2003**, *46*, 115–123.
8. D'Amato, R. J.; Loughnan, M. S.; Flynn, E.; Folkman, J. *Proc. Natl. Acad. Sci. U.S.A.* **1994**, *91*, 4082–4085.
9. Zhang, Y.; Griffith, E. C.; Sage, J.; Jacks, T.; Liu, J. O. *Proc. Natl. Acad. Sci. U.S.A.* **2000**, *97*, 6427–6432.
10. Jia, M. C.; Schwartz, M. A.; Sang, Q. A. *Adv. Exp. Med. Biol.* **2000**, *476*, 181–194.
11. Bergers, G.; Song, S.; Meyer-Morse, N.; Bergsland, E.; Hanahan, D. *J. Clin. Invest.* **2003**, *111*, 1287–1295.
12. Kakeya, H.; Onose, R.; Koshino, H.; Yoshida, A.; Kobayashi, K.; Kageyama, S.-I.; Osada, H. *J. Am. Chem. Soc.* **2002**, *124*, 3496–3497.
13. Kakeya, H.; Onose, R.; Yoshida, A.; Koshino, H.; Osada, H. *J. Antibiot.* **2002**, *55*, 829–831.
14. Shoji, M.; Yamaguchi, J.; Kakeya, H.; Osada, H.; Hayashi, Y. *Angew. Chem. Int. Ed.* **2002**, *41*, 3192–3194.
15. Shoji, M.; Kishida, S.; Takeda, M.; Kakeya, H.; Osada, H.; Hayashi, Y. *Tetrahedron Lett.* **2002**, *43*, 9155–9158.
16. Asami, Y.; Kakeya, H.; Onose, R.; Yoshida, A.; Matsuzaki, H.; Osada, H. *Org. Lett.* **2002**, *4*, 2845–2848.
17. Hayashi, Y.; Shoji, M.; Yamaguchi, J.; Sato, K.; Yamaguchi, S.; Mukaiyama, T.; Sakai, K.; Asami, Y.; Kakeya, H.; Osada, H. *J. Am. Chem. Soc.* **2002**, *124*, 12078–12079.
18. Marui, S.; Kishimoto, S. *Chem. Pharm. Bull.* **1992**, *40*, 575–579.

19. Turk, B. E.; Su, Z.; Liu, J. O. *Bioorg. Med. Chem.* **1998**, *6*, 1163–1169.
20. Bollinger, P.; Sigg, H. P.; Weber, H. P. *Helv. Chim. Acta* **1973**, *56*, 819–830.
21. Marui, S.; Itoh, F.; Kozai, Y.; Sudo, K.; Kishimoto, S. *Chem. Pharm. Bull.* **1992**, *40*, 96–101.
22. Sun, L.; Tran, N.; Tang, F.; App, H.; Hirth, P.; Mcmahon, G.; Tang, C. *J. Med. Chem.* **1998**, *41*, 2588–2603.
23. Griffith, E. C.; Su, Z.; Turk, B. E.; Chen, S.; Chang, Y.-H.; Wu, Z.; Biemann, K.; Liu, J. O. *Chem. Biol.* **1997**, *4*, 461–471.
24. Griffith, E. C.; Su, Z.; Niwayama, S.; Ramsay, C. A.; Chang, Y.-H.; Liu, J. O. *Proc. Natl. Acad. Sci. U.S.A.* **1998**, *95*, 15183–15188.
25. Sin, N.; Meng, L.; Wang, M. Q. W.; Wen, J. J.; Bornmann, W. G.; Crews, C. M. *Proc. Natl. Acad. Sci. U.S.A.* **1997**, *94*, 6099–6103.
26. Li, X.; Chang, Y.-H. *Proc. Natl. Acad. Sci. U.S.A.* **1995**, *92*, 12357–12361.
27. Ben-Bassat, A.; Bauer, K.; Chang, S.-Y.; Myambo, K.; Boosman, A.; Chang, S. *J. Bacteriol.* **1987**, *169*, 751–757.
28. Chang, Y.-H.; Teichert, U.; Smith, J. A. *J. Biol. Chem.* **1990**, *265*, 19892–19897.
29. Arfin, S. M.; Kendall, R. L.; Hall, L.; Weaver, L. H.; Stewart, A. E.; Matthews, B. W.; Bradshaw, R. A. *Proc. Natl. Acad. Sci. U.S.A.* **1995**, *92*, 7714–7718.
30. Liu, S.; Widom, J.; Kemp, C. W.; Crews, C. M.; Clardy, J. *Science* **1998**, *282*, 1324–1327.
31. Twardowski, P.; Gradishar, W. J. *Curr. Opin. Oncol.* **1997**, *9*, 584–589.
32. Figg, W. D.; Kruger, E. A.; Price, D. K.; Kim, S.; Dahut, W. D. *Invest. New Drugs* **2002**, *20*, 183–194.
33. Turk, B. E.; Griffith, E. C.; Wolf, S.; Biemann, K.; Chang, Y.-H.; Liu, J. O. *Chem. Biol.* **1999**, *6*, 823–833.
34. Yeh, J.-R. J.; Mohan, R.; Crews, C. M. *Proc. Natl. Acad. Sci. U.S.A.* **2000**, *97*, 12782–12787.
35. Placidi, L.; Cretton-Scott, E.; de Sousa, G.; Rahmani, R.; Placidi, M.; Sommadossi, J. P. *Cancer Res.* **1995**, *55*, 3036–3042.
36. Herbst, R. S.; Madden, T. L.; Tran, H. T.; Blumenschein, Jr. G. R.; Meyer, C. A.; Seabrooke, L. F.; Khuri, F. R.; Puduvalli, V. K.; Allgood, V.; Fritsche, Jr. H. A.; Hinton, L.; Newman, R. A.; Crane, E. A.; Fossella, F. V.; Dordal, M.; Goodin, T.; Hong, W. K. *J. Clin. Oncol.* **2002**, *20*, 4440–4447.

ECH, an Epoxycyclohexenone Derivative That Specifically Inhibits Fas Ligand-Dependent Apoptosis in CTL-Mediated Cytotoxicity[1]

Tomokazu Mitsui,* Yasunobu Miyake,*† Hideaki Kakeya,† Hiroyuki Osada,† and Takao Kataoka[2]*

CTL eliminate cells infected with intracellular pathogens and tumor cells by two distinct mechanisms mediated by Fas ligand (FasL) and lytic granules that contain perforin and granzymes. In this study we show that an epoxycyclohexenone derivative, (*2R,3R,4S*)-2,3-epoxy-4-hydroxy-5-hydroxymethyl-6-(*1E*)-propenyl-cyclohex-5-en-1-one (ECH) specifically inhibits the FasL-dependent killing pathway in CTL-mediated cytotoxicity. Recently, we have reported that ECH blocks activation of procaspase-8 in the death-inducing signaling complex and thereby prevents apoptosis induced by anti-Fas Ab or soluble FasL. Consistent with this finding, ECH profoundly inhibited Fas-mediated DNA fragmentation and cytolysis of target cells induced by perforin-negative mouse CD4$^+$ CTL and alloantigen-specific mouse CD8$^+$ CTL pretreated with an inhibitor of vacuolar type H$^+$-ATPase concanamycin A that selectively induces inactivation and proteolytic degradation of perforin in lytic granules. However, ECH barely influenced perforin/granzyme-dependent DNA fragmentation and cytolysis of target cells mediated by alloantigen-specific mouse CD8$^+$ CTL. The components of lytic granules and the granule exocytosis pathway upon CD3 stimulation were also insensitive to ECH. In conclusion, our present results demonstrate that ECH is a specific nonpeptide inhibitor of FasL-dependent apoptosis in CTL-mediated cytotoxicity. Therefore, ECH can be used as a bioprobe to evaluate the contributions of two distinct killing pathways in various CTL-target settings. *The Journal of Immunology*, 2004, 172: 3428–3436.

Cytotoxic T lymphocytes play a critical role in protection against intracellular pathogens and tumor cells as well as autoimmunity and transplant rejection. To induce apoptosis of target cells, CTL mainly use two distinct pathways that are dependent on Fas ligand (FasL)[3] and lytic granules that contain the pore-forming protein perforin and serine proteases termed granzymes (1, 2). CD8$^+$ CTL eliminate target cells primarily via the perforin-dependent pathway, whereas the FasL-dependent killing pathway is dominantly used by CD4$^+$ CTL (1). The perforin system is essential for the control of viral infection and tumor rejection, and the Fas/FasL system is important for lymphocyte homeostasis (1, 3–5). However, these two killing systems play different regulatory roles in various physiological and pathogenic situations.

CTL harbor lytic granules that store perforin and granzymes under the acidic environment (6). Upon TCR stimulation, CTL rapidly release lytic granules into the interface between CTL-target conjugates (1, 2). Perforin facilitates the translocation of granzymes A and B into the cytosol without pore formation on the plasma membrane (7). Granzymes A and B are major molecules that induce target cell death (1, 2). Granzyme B initiates caspase-dependent apoptosis that requires the release of proapoptotic mitochondrial factors (8–10). By contrast, granzyme A triggers a caspase-independent alternate cell death pathway characterized by ssDNA nicks (11, 12). However, in the granule-mediated killing pathway, granzyme B is critical for rapid induction of DNA fragmentation in target cells (13).

Upon TCR stimulation, FasL is newly synthesized and then transported to the cell surface of CTL (1). In the cytoplasmic region, Fas contains the death domain that is required for interaction with the adaptor protein Fas-associated death domain protein (FADD) (3–5). Membrane-bound FasL triggers Fas oligomerization, which allows the recruitment of FADD to the Fas death domain (3–5). FADD subsequently binds to procaspase-8 via the mutual interaction of their death effector domain, resulting in the formation of death-inducing signaling complex (DISC) (14). In the DISC, procaspase-8 immediately dimerizes and undergoes self-cleavage, generating the active heterotetramer composed of two large subunits and two small subunits (15, 16). Active caspase-8 cleaves downstream substrates such as procaspase-3 or Bid, essential for apoptosis execution (1–5).

Membrane-permeable small compounds are expected to be valuable tools to clarify the molecular basis of complex intracellular signaling pathways and to be potential therapeutic drugs as well. Hence, specific modulators of CTL-mediated cytotoxicity are highly useful. Previously, we reported that vacuolar type H$^+$-ATPase inhibitor concanamycin A (CMA) is a specific inhibitor of the perforin-dependent killing pathway in target cell lysis mediated by CTL and NK cells (17, 18). However, the FasL-dependent killing pathway is totally insensitive to CMA (18). CMA perturbs acidification of lytic granules and raises

*Division of Bioinformatics, Center for Biological Resources and Informatics, Tokyo Institute of Technology, Yokohama, Japan; and †Antibiotics Laboratory, Discovery Research Institute, RIKEN, Saitama, Japan

Received for publication July 28, 2003. Accepted for publication January 7, 2004.

The costs of publication of this article were defrayed in part by the payment of page charges. This article must therefore be hereby marked *advertisement* in accordance with 18 U.S.C. Section 1734 solely to indicate this fact.

[1] This work was supported by a grant-in-aid for scientific research from the Ministry of Education, Culture, Sports, Science, and Technology and research grants from Kato Memorial Bioscience Foundation and Mitsubishi Pharma Research Foundation. Y.M. was partly supported by the Grant of the 21st Century COE Program, Ministry of Education, Culture, Sports, Science and Technology.

[2] Address correspondence and reprint requests to Dr. Takao Kataoka, Division of Bioinformatics, Center for Biological Resources and Informatics, Tokyo Institute of Technology, 4259 Nagatsuta-cho, Midori-ku, Yokohama 226-8501, Japan. E-mail address: tkataoka@bio.titech.ac.jp

[3] Abbreviations used in this paper: FasL, Fas ligand; FADD, Fas-associated death domain protein; DISC, death-inducing signaling complex; CMA, concanamycin A; ECH, (*2R,3R,4S*)-2,3-epoxy-4-hydroxy-5-hydroxymethyl-6-(*1E*)-propenyl-cyclohex-5-en-1-one; FADD, Fas-associated death domain protein; KLH, keyhole limpet hemocyanin; PCA, penicillic acid.

0022-1767/04/$02.00

the internal pH to around neutral (19). Neutralization of acidic pH induces inactivation of perforin in a Ca^{2+}-dependent manner and subsequent proteolytic degradation of perforin by serine proteases (17, 20). To date, CMA has been frequently used to evaluate the contribution of the perforin-dependent killing pathway in cell-mediated cytotoxicity.

The early signal transduction of Fas-mediated apoptosis is a complex process regulated by various cellular proteins exerting proapoptotic and antiapoptotic functions. To search for specific modulators of Fas-mediated apoptosis, we have screened natural products, such as microbial metabolites, and identified several modulators that block or enhance the Fas death signals (21–24). It was reported that an epoxycyclohexenone derivative, (*2R,3R,4S*)-2,3-epoxy-4-hydroxy-5-hydroxymethyl-6-(*1E*)-propenyl-cyclohex-5-en-1-one (ECH; see Fig. 1*A*), prevents Fas-mediated apoptosis (25). However, the molecular target of ECH remained to be elucidated. Recently, we have shown that ECH inhibits apoptosis mediated by Fas and TNF receptor 1 through preventing activation of procaspase-8 in the DISC (24). By contrast, death receptor-independent apoptosis induced by chemical drugs and UV irradiation was totally insensitive to ECH (24). In the present report we have studied the inhibitory effects of ECH on two distinct CTL-mediated killing pathways. Our results demonstrate that ECH does not affect the perforin-dependent killing pathway, but selectively inhibits the FasL-dependent killing pathway mediated by Ag-specific CTL.

Materials and Methods

Cells

The H-2^d-specific $CD8^+$ CTL clone OE4 (26) and the keyhole limpet hemocyanin (KLH)-specific H-2^d (I-E^d)-restricted $CD4^+$ CTL clone BK-1 (27) were maintained in RPMI 1640 medium (Invitrogen, Carlsbad, CA) supplemented with 10% (v/v) heat-inactivated FCS (JRH Biosciences, Lenexa, KS), 50 μM 2-ME, 5% (v/v) rat spleen cell-conditioned medium (culture supernatant of rat spleen cells stimulated with 5 μg/ml CMA for 24 h), and penicillin-streptomycin-neomycin antibiotic mixture (Invitrogen). OE4 cells were stimulated with mitomycin C-treated spleen cells prepared from BALB/c mice every 2 wk. BK-1 cells were stimulated with 10 μg/ml KLH (Calbiochem, Darmstadt, Germany) in the presence of mitomycin C-treated BALB/c mouse spleen cells every 2 wk. BALB/c mouse-derived B lymphoma (A20, A20.HL, A20.FO) were maintained in RPMI 1640 medium containing 10% (v/v) FCS, 50 μM 2-ME, and penicillin-streptomycin-neomycin antibiotic mixture. A20.HL cells were the BALB/c B lymphoma transfected with L and H chain genes of anti-TNP IgM Ab (28). A20.FO cells were the Fas-negative variant subcloned from the Fas-positive parent cell line A20.2J (18). DBA/2 mouse-derived T lymphoma L5178Y and the Fas-expressing transfectant of L5178Y (L5178Y-Fas) (29) were maintained in RPMI 1640 medium containing 10% (v/v) FCS, 50 μM 2-ME, and penicillin-streptomycin-neomycin antibiotic mixture.

Reagents

ECH was isolated from the culture broth of a producing fungal strain using a bioassay-guided purification procedure (24). CMA was purchased from Wako Pure Chemical Industries (Osaka, Japan). Recombinant human soluble FasL was a gift from Dr. J. Tschopp (Institute of Biochemistry, University of Lausanne, Epalinges, Switzerland) and was used as described previously (30).

DNA fragmentation assay

Target cells were labeled with 37 kBq of [^{3}H]TdR (ICN Biomedicals, Costa Mesa, CA) for 16 h and washed three times before use. The labeled cells (1×10^5 cells/ml, 100 μl) were preincubated with the indicated concentrations of ECH for 1 or 2 h, then mixed with 100 μl of CTL in U-bottom, 96-well microtiter plates. The plates were centrifuged ($300 \times g$, 3 min) and then incubated for 4 h. The drug concentration during coculture with CTL was diluted into half the initial drug concentration. At the end of the culture, 10 μl of 2% Triton X-100 was added to each well, and the cells were lysed by pipetting, followed by centrifugation ($600 \times g$, 5 min). One hundred microliters of supernatants were harvested and measured for radioactivity. Specific ^{3}H-labeled DNA release (percentage) was calculated using the following formula: (experimental cpm − spontaneous cpm)/(maximum cpm − spontaneous cpm) × 100.

^{51}Cr release assay

Target cells were labeled with 1850 kBq of [^{51}Cr]sodium chromate (Amersham Biosciences, Piscataway, NJ) in 100 μl of 50% (v/v) FCS for 1 h and washed three times with the medium. The labeled cells (1×10^5 cells/ml, 100 μl) were preincubated with indicated concentrations of ECH for 1 h, then mixed with 100 μl of CTL in U-bottom, 96-well microtiter plates. The plates were centrifuged ($300 \times g$, 3 min) and then incubated for 4 h. One hundred microliters of supernatants were harvested and measured for radioactivity. Specific ^{51}Cr release (percentage) was calculated using the following formula: (experimental cpm − spontaneous cpm)/(maximum cpm − spontaneous cpm) × 100.

Analysis of effector/target conjugate formation

Analysis of conjugate formation was performed as described previously (31). Target cells (5×10^5 cells/ml) were treated with or without ECH for 1 h, then stained with 62.5 μg/ml hydroethidine (Polysciences, Warrington, PA) for 30 min on ice. Effector cells (5×10^5 cells/ml) were stained with 0.25 μM calcein-AM (Molecular Probes, Eugene, OR) for 30 min on ice. Both types of stained cells (5×10^5 cells/ml, 250 μl) were washed twice with the medium, then transferred in a single tube. The cell mixtures were either left untreated or centrifuged ($300 \times g$, 3 min), then incubated at 25°C for 30 min. The cells were resuspended carefully by pipetting and immediately analyzed by FACS.

Western blotting

OE4 cells (1×10^6 cells) were washed with PBS and lysed with 1% Triton X-100, 50 mM Tris-HCl (pH 7.4), and protease inhibitor mixture (Complete; Roche, Mannheim, Germany) on ice for 15 min. After centrifugation ($10{,}000 \times g$, 5 min), supernatants were collected. Postnuclear lysates (30 μg/lane) were separated by 10% SDS-PAGE and analyzed by Western blotting using ECL detection reagents (Amersham Biosciences). Anti-mouse perforin Ab P1-8 (32) was provided by Dr. H. Yagita (Juntendo University School of Medicine, Tokyo, Japan).

Measurement of granzyme activity

OE4 cells (1×10^6 cells) were washed with PBS and lysed with 0.5% Triton X-100, 10 mM HEPES-NaOH (pH 7.4), 150 mM NaCl, 1 mM $CaCl_2$, and 1 mM $MgCl_2$ on ice for 15 min. After centrifugation ($10{,}000 \times g$, 5 min), supernatants were collected. Postnuclear lysates (5 μg) were incubated with 200 μl of the reaction mixture (200 μM 5,5′-dithio-bis-(2-nitrobenzoic acid) plus either 200 μM CBZ-Gly-Arg-thiobenzylester for the granzyme A substrate or Boc-Ala-Ala-Asp-thiobenzylester for the granzyme B substrate (Enzyme Systems Products, Dublin, CA) in 10 mM HEPES-NaOH (pH 7.4), 150 mM NaCl, 1 mM $CaCl_2$, and 1 mM $MgCl_2$) at room temperature. Absorbance at 415 nm was measured.

Analysis of granule exocytosis

OE4 cells (1×10^6 cells/ml, 100 μl) were transferred into 96-well microtiter plates coated with anti-mouse CD3 Ab 145-2C11 (10 μg/ml). After centrifugation ($300 \times g$, 3 min), the cells were incubated for 4 h. Culture supernatants were removed and measured for the activity of granzyme A as described above.

Results

ECH inhibits DNA fragmentation induced by soluble FasL

B lymphoma A20 cells are sensitive to Fas-mediated apoptosis and exhibited DNA fragmentation characteristic of apoptosis within 4 h upon exposure to cross-linked FasL, whereas Fas-negative A20.FO cells were totally resistant to cross-linked FasL (Fig. 1*B*). ECH inhibited FasL-induced DNA fragmentation in a dose-dependent manner, and complete inhibition was observed when A20 cells were pretreated with 50–100 μM ECH for 1 h (Fig. 1*C*). ECH was only diluted into half of the initial concentration during exposure to FasL, because DNA fragmentation was partially reversed when ECH was removed from A20 cells during the coculture with FasL (Fig. 1*D*). Under these experimental conditions, ECH was not cytotoxic to the cell, as no DNA fragmentation was induced by ECH alone (Fig. 1*D*). Twenty-four-hour incubation of A20 cells with ECH resulted in a marked reduction of live cell-number without an induction of DNA fragmentation (Fig. 1, *E* and

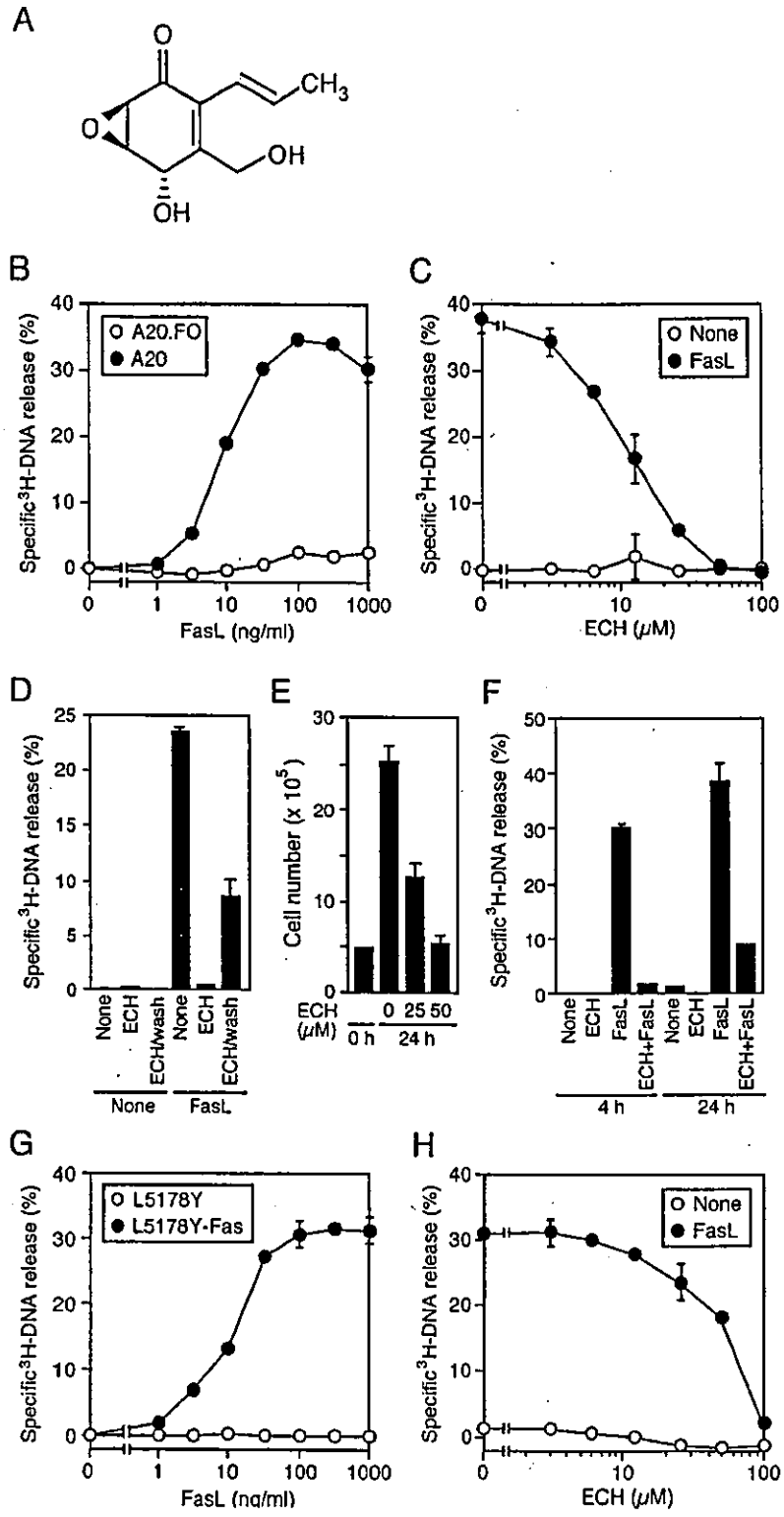

FIGURE 1. ECH inhibits DNA fragmentation induced by soluble FasL. *A*, Structure of ECH. *B–D*, [^{3}H]TdR-labeled A20 (●) and A20.FO (O) cells were incubated with various concentrations of cross-linked FasL for 4 h (*B*). [^{3}H]TdR-labeled A20 cells were preincubated with serial dilutions of ECH for 1 h, and then incubated with (●) or without (O) cross-linked FasL (50 ng/ml) for 4 h (*C*). [^{3}H]TdR-labeled A20 cells were preincubated with or without ECH (50 μM) for 1 h and either untreated or washed with the medium to remove ECH, followed by incubation with or without cross-linked FasL (50 ng/ml) for 4 h (*D*). The radioactivity of fragmented DNA was measured. Data points represent the mean ± SD of triplicate cultures. *E*, A20 cells were incubated in the presence of the indicated concentrations of ECH for 24 h. The number of live cells was counted by trypan blue dye exclusion. Data points represent the mean ± SD of triplicate determinations. *F–H*, [^{3}H]TdR-labeled A20 cells were preincubated with or without ECH (50 μM) for 1 h, and then incubated in the presence or the absence of cross-linked FasL (50 ng/ml) for 4 or 24 h (*F*). [^{3}H]TdR-labeled L5178Y-Fas (●) and L5178Y (O) cells were incubated with various concentrations of cross-linked FasL for 4 h (*G*). [^{3}H]TdR-labeled L5178Y-Fas cells were preincubated with serial dilutions of ECH for 2 h and then incubated with (●) or without (O) cross-linked FasL (50 ng/ml) for 4 h (*H*). The radioactivity of fragmented DNA was measured. Data points represent the mean ± SD of triplicate cultures.

F). Less than 20% of the total cells were stained with trypan blue when A20 cells were treated with 50 μM ECH for 24 h (data not shown). In addition to A20 cells, the T lymphoma L5178Y cells were used for the second cell line to study the biological activity of ECH. Although L5178Y cells were insensitive to cross-linked FasL, Fas-transfected L5178Y cells (L5178Y-Fas) were highly susceptible to cross-linked FasL (Fig. 1*G*). DNA fragmentation induced by cross-linked FasL was completely inhibited when L5178Y-Fas cells were pretreated with 100 μM ECH for 2 h, and ECH alone did not induce DNA fragmentation (Fig. 1*H*).

ECH inhibits FasL-dependent DNA fragmentation mediated by perforin-negative CD4$^+$ CTL

KLH-specific H-2^d-restricted CD4$^+$ CTL clone BK-1 cells are perforin-negative (33), and the killing pathway of this clone is exclusively dependent on FasL (29). BK-1 cells induced DNA

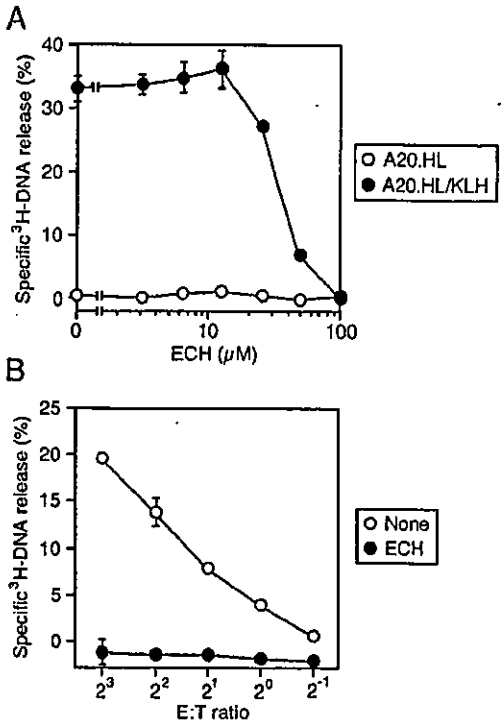

FIGURE 2. ECH inhibits FasL-based DNA fragmentation mediated by the CD4$^+$ CTL clone. *A*, [^{3}H]TdR-labeled A20.HL cells were pulsed with or without KLH (300 μg/ml) before assay. KLH-pulsed A20.HL (●) and nonpulsed A20.HL (○) cells were preincubated with serial dilutions of ECH for 1 h. The target cells were mixed with BK-1 cells (E:T cell ratio = 8), and then incubated for 4 h. *B*, [^{3}H]TdR-labeled KLH-pulsed A20.HL cells were preincubated with (●) or without (○) 100 μM ECH for 1 h. The target cells were mixed with different numbers of BK-1 cells and then incubated for 4 h. The radioactivity of fragmented DNA was measured. Data points represent the mean ± SD of triplicate cultures.

fragmentation in KLH-pulsed A20.HL cells, but not A20.HL cells without Ag (Fig. 2*A*). ECH markedly inhibited DNA fragmentation induced by BK-1 cells when KLH-pulsed A20.HL cells were pretreated with 50–100 μM for 1 h (Fig. 2).

To exclude the possibility that ECH pretreatment of target cells decreases CTL-target interaction, ECH-pretreated A20.HL cells were mixed with BK-1 cells, and resultant conjugate formation was analyzed by FACS (Fig. 3*A*). A brief centrifugation facilitated the formation of CTL-target conjugates. ECH did not influence conjugate formation at 50 μM. It should be noted that this concentration resulted in a profound inhibition of DNA fragmentation induced by BK-1 cells (Fig. 2*A*). As a slight reduction of CTL-target conjugates was observed when A20.HL cells were pretreated with 100 μM ECH, ECH might affect the interaction between CTL and target cells at higher concentrations.

ECH does not affect the components of lytic granules and granule exocytosis in CD8$^+$ CTL

The H-2^d-specific CD8$^+$ CTL clone OE4 cells kill target cells via both the perforin-dependent pathway and the FasL-dependent pathway (18). As observed with BK-1 cells, ECH did not substantially prevent conjugate formation between OE4 and A20 cells up to 50 μM (Fig. 3*B*). Perforin and granzymes stored in lytic granules are released upon TCR activation and induce apoptosis in target cells. The cellular levels of perforin and granzymes were thus analyzed in OE4 cells exposed to ECH. In contrast to CMA that induced a marked reduction of perforin, ECH failed to decrease the cellular amount of perforin in OE4 cells (Fig. 4*A*). The enzyme activities of granzymes A and B in ECH-treated OE4 cells were also unimpaired (Fig. 4*B*). Stimulation of OE4 cells with plate-coated anti-CD3 Ab induced exocytosis of lytic granules into the culture medium, and ECH only marginally reduced granule exocytosis even at 50 μM (Fig. 4*C*). In our experimental system,

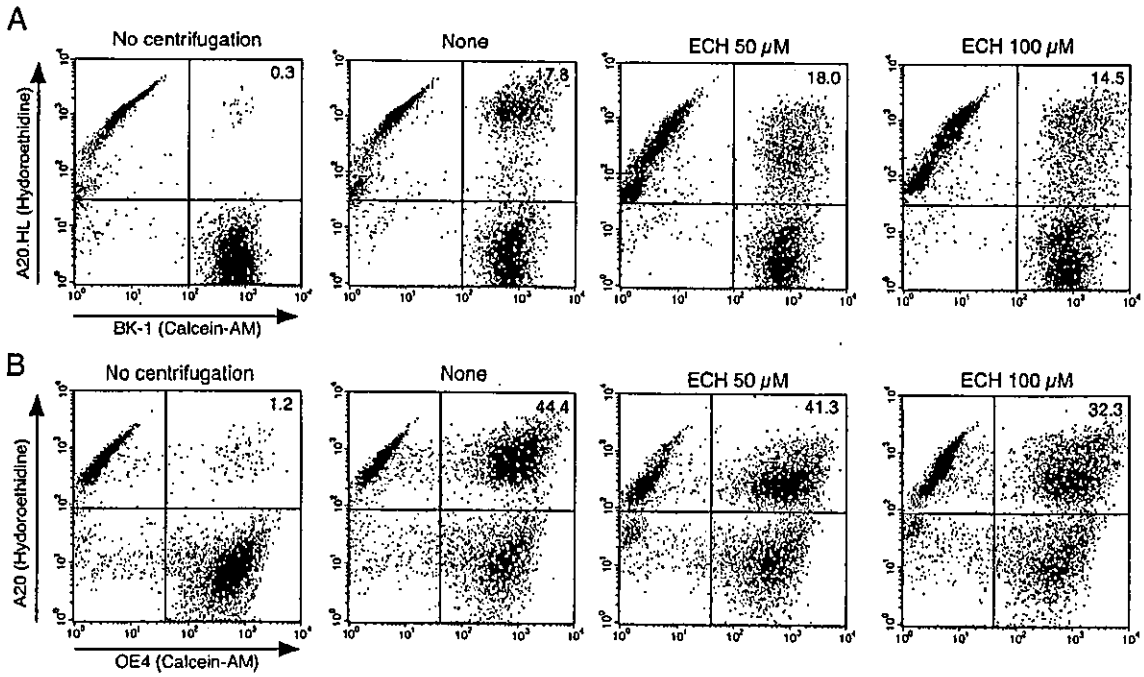

FIGURE 3. Effect of ECH on conjugate formation between CTL and target cells. *A*, Hydroethidine-stained A20.HL cells were treated with the indicated concentrations of ECH for 1 h, then mixed with calcein-AM-stained BK-1 cells in a single tube. The cells were either left untreated (*left panel*) or briefly centrifuged (*other panels*), and then incubated at 25°C for 30 min. *B*, Hydroethidine-stained A20 cells were treated with the indicated concentrations of ECH for 1 h, then mixed with calcein-AM-stained OE4 cells in a single tube. The cells were either left untreated (*left panel*) or briefly centrifuged (*other panels*), then incubated at 25°C for 30 min. Conjugate formation was analyzed by FACS.

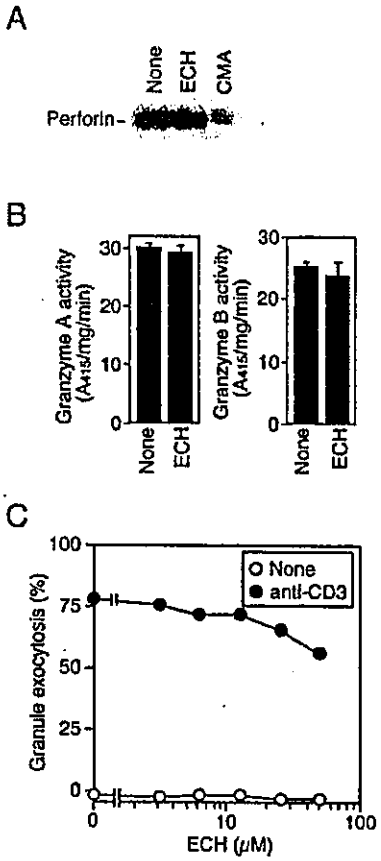

FIGURE 4. Effect of ECH on the components of lytic granules and granule exocytosis. *A*, OE4 cells were treated with 50 μM ECH or 100 nM CMA for 4 h or were left untreated. Postnuclear lysates were analyzed by Western blotting using anti-perforin Ab. *B*, OE4 cells were treated with or without 50 μM ECH for 4 h. Postnuclear lysates were measured for the enzyme activity of granzymes A and B. *C*, OE4 cells were incubated with (●) or without (○) immobilized anti-CD3 Ab in the presence of serial dilutions of ECH for 4 h. Culture supernatants were measured for the granzyme A activity. Data points represent the mean ± SD of triplicate cultures.

effector CTL were exposed to ECH at half the initial concentrations for pretreatment of target cells. To avoid any direct effects on lytic granules and the granule exocytosis pathway during the killing assay, ECH was used at concentrations <100 μM for pretreatment of target cells.

ECH does not inhibit perforin-dependent DNA fragmentation mediated by CD8⁺ CTL

To determine whether ECH inhibits perforin-dependent DNA fragmentation, two different Fas-negative lymphomas were used as target cells against OE4 cells. As shown in Fig. 1, A20.FO and L5178Y cells were completely resistant to soluble FasL. Therefore, DNA fragmentation of these target cells induced by OE4 cells is solely dependent on the perforin/granzyme system. ECH did not affect DNA fragmentation of A20.FO cells (Fig. 5, *A* and *B*) and L5178Y cells (Fig. 5*C*) at concentrations up to 50 μM. Only slight reduction of DNA fragmentation was observed when A20.FO cells (Fig. 5*A*) and L5178Y cells (Fig. 5, *C* and *D*) were pretreated with 100 μM ECH.

ECH inhibits FasL-dependent DNA fragmentation mediated by CD8⁺ CTL

Fas-positive target cells are killed by OE4 cells via the perforin-dependent pathway and the FasL-dependent pathway. To block the perforin-dependent killing pathway, OE4 cells were pretreated with 100 nM CMA for 2 h. ECH alone did not affect DNA fragmentation of Fas-positive A20 cells induced by OE4 cells (Fig. 6, *A* and *B*). However, FasL-dependent DNA fragmentation induced by CMA-treated OE4 cells was prevented by ECH in a dose-dependent manner, and ECH completely inhibited DNA fragmentation when A20 cells were pretreated with 50 μM (Fig. 6, *A* and *B*). These results demonstrate that ECH inhibits FasL-dependent DNA fragmentation mediated by CD8⁺ CTL, but not perforin/granzyme-dependent DNA fragmentation. Likewise, in L5178Y-Fas cells, ECH dose-dependently inhibited DNA fragmentation induced by CMA-treated OE4 cells, and complete inhibition was observed when L5178Y-Fas cells were pretreated with 100 μM ECH (Fig. 6, *C* and *D*). The CMA-insensitive killing of OE4 cells corresponded to 40 and 70% in A20 cells (Fig. 6*B*) and L5178Y-Fas cells (Fig. 6*D*), respectively, suggesting that the FasL-dependent killing pathway plays a more dominant role in the induction of apoptosis in L5178Y-Fas cells than A20 cells. This difference might explain the observation that ECH alone exerts a stronger inhibitory activity toward DNA fragmentation of L5178Y-Fas cells.

ECH inhibits FasL-dependent DNA fragmentation, but not perforin-dependent DNA fragmentation, mediated by alloantigen-specific bulk CTL

To generalize the selective inhibitory effects of ECH on FasL-dependent DNA fragmentation, alloantigen-specific bulk CTL were induced by in vitro MLC for 4 days and used as effector CTL. In agreement with the observations using OE4 cells, ECH barely influenced DNA fragmentation of A20.FO cells induced by MLC cells (Fig. 7, *A* and *B*). In Fas-positive A20 cells, FasL-dependent DNA fragmentation induced by CMA-treated MLC cells was almost completely inhibited by ECH at 25 μM (Fig. 7*C*). By contrast, ECH alone did not significantly influence DNA fragmentation induced by MLC cells under these conditions (Fig. 7, *C* and *D*).

ECH inhibits FasL-dependent target cell lysis, but not perforin-dependent target cell lysis, in CTL-mediated cytotoxicity

The ^{51}Cr release assay has been widely used for the measurement of target cell lysis in CTL-mediated cytotoxicity. As observed with the DNA fragmentation assay (Fig. 1*C*), ECH inhibited cytolysis of A20 cells induced by soluble FasL in a dose-dependent manner (Fig. 8*A*). Consistent with this observation, ECH strongly prevented FasL-dependent target cell lysis mediated by BK-1 cells (Fig. 8*B*) as well as OE4 cells pretreated with CMA (Fig. 8*C*). By contrast, perforin-dependent target cell lysis mediated by OE4 cells was only marginally affected by ECH (Fig. 8*D*).

Discussion

Recently, we have shown that ECH inhibits Fas-mediated apoptosis by blocking activation of procaspase-8 in the DISC (24). In this work we have investigated whether ECH inhibits the perforin-dependent killing pathway and the FasL-dependent killing pathway in CTL-mediated cytotoxicity. In the short term killing assay based on two different murine Fas-positive/negative target cells vs the CD4⁺ and CD8⁺ CTL clones as well as alloantigen-specific bulk MLC cells, ECH profoundly blocked the FasL-dependent DNA fragmentation and cytolysis of target cells, but barely prevented the perforin/granzyme-dependent DNA fragmentation and cytolysis of target cells. Moreover, ECH did not influence the cellular levels of perforin and granzymes A/B and only marginally reduced the granule exocytosis pathway in response to CD3 stimulation.

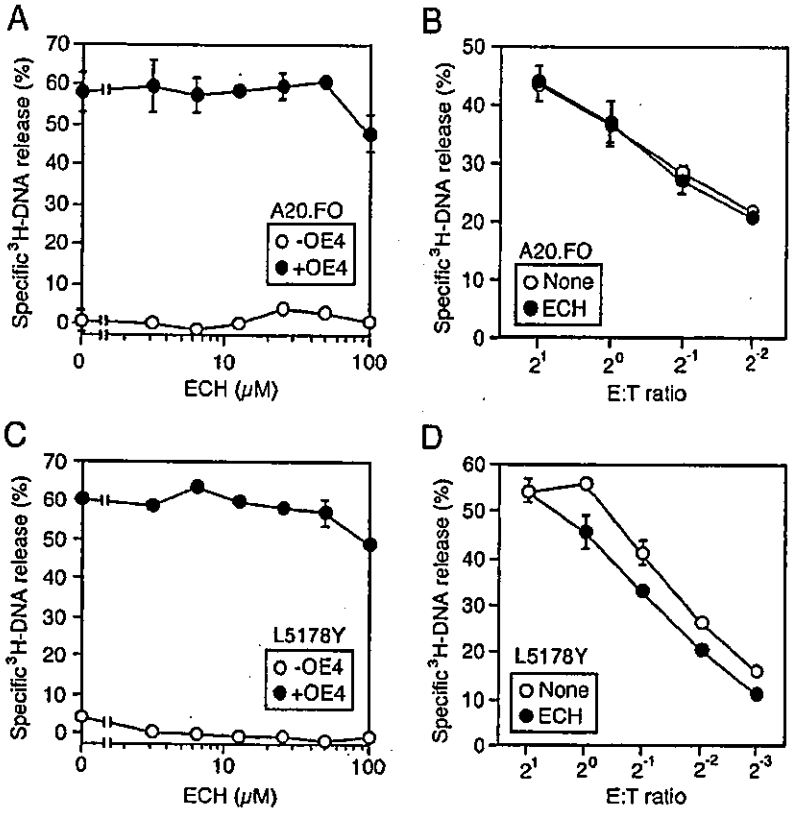

FIGURE 5. ECH does not affect perforin-based DNA fragmentation mediated by the $CD8^+$ CTL clone. *A*, [^{3}H]TdR-labeled A20.FO cells were pretreated with serial dilutions of ECH for 1 h. The target cells were mixed with (●) or without (O) OE4 cells (E:T cell ratio = 2), then incubated for 4 h. *B*, [^{3}H]TdR-labeled A20.FO cells were pretreated with (●) or without (O) 50 μM ECH for 1 h. The target cells were mixed with different numbers of OE4 cells, then incubated for 4 h. *C*, [^{3}H]TdR-labeled L5178Y cells were pretreated with serial dilutions of ECH for 2 h. The target cells were mixed with (●) or without (O) OE4 cells (E:T cell ratio = 2), then incubated for 4 h. *D*, [^{3}H]TdR-labeled L5178Y cells were pretreated with (●) or without (O) 100 μM ECH for 2 h. The target cells were mixed with different numbers of OE4 cells, then incubated for 4 h. The radioactivity of fragmented DNA was measured. Data points represent the mean ± SD of triplicate cultures.

Thus, our present results demonstrate that ECH is a highly selective inhibitor to block the FasL-dependent killing pathway in CTL-mediated cytotoxicity.

Death receptor-independent apoptosis induced by chemical compounds (i.e., staurosporine, MG-132, and ceramide) and UV irradiation was insensitive to ECH, whereas ECH markedly inhibited apoptosis induced by anti-Fas Ab, FasL, or TNF (24). These results suggest that ECH selectively blocks death receptor-mediated apoptosis that requires activation of procaspase-8. In the granule-dependent killing pathway, granzymes A and B have major roles in inducing target cell death upon translocation into the cytosol (1, 2). Granzyme A induces a caspase-independent cell death

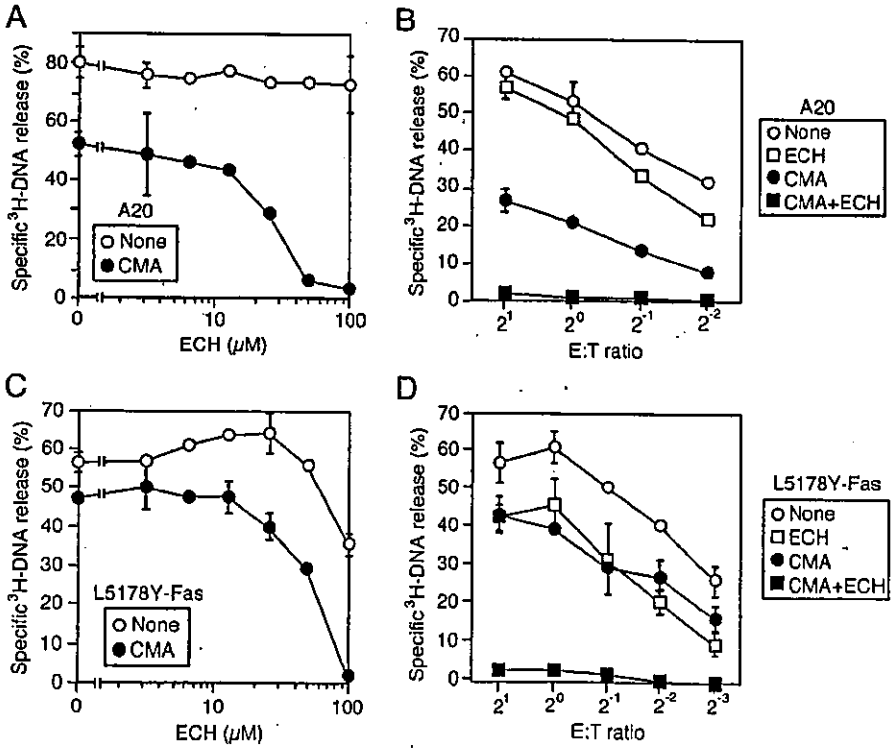

FIGURE 6. ECH selectively blocks FasL-based DNA fragmentation mediated by the $CD8^+$ CTL clone. *A*, OE4 cells were pretreated with (●) or without (O) 100 nM CMA for 2 h. [^{3}H]TdR-labeled A20 cells were pretreated with serial dilutions of ECH for 1 h. The target cells were mixed with OE4 cells (E:T cell ratio = 2), then incubated for 4 h. *B*, OE4 cells were pretreated with (● and ■) or without (O and □) 100 nM CMA for 2 h. [^{3}H]TdR-labeled A20 cells were pretreated with (□ and ■) or without (O and ●) 50 μM ECH for 1 h. The target cells were mixed with different numbers of OE4 cells, then incubated for 4 h. *C*, OE4 cells were pretreated with (●) or without (O) 100 nM CMA for 2 h. [^{3}H]TdR-labeled L5178Y-Fas cells were pretreated with serial dilutions of ECH for 2 h. The target cells were mixed with OE4 cells (E:T cell ratio = 2), then incubated for 4 h. *D*, OE4 cells were pretreated with (● and ■) or without (O and □) 100 nM CMA for 2 h. [^{3}H]TdR-labeled L5178Y-Fas cells were pretreated with (□ and ■) or without (O and ●) 100 μM ECH for 2 h. The target cells were mixed with different numbers of OE4 cells, then incubated for 4 h. The radioactivity of fragmented DNA was measured. Data points represent the mean ± SD of triplicate cultures.

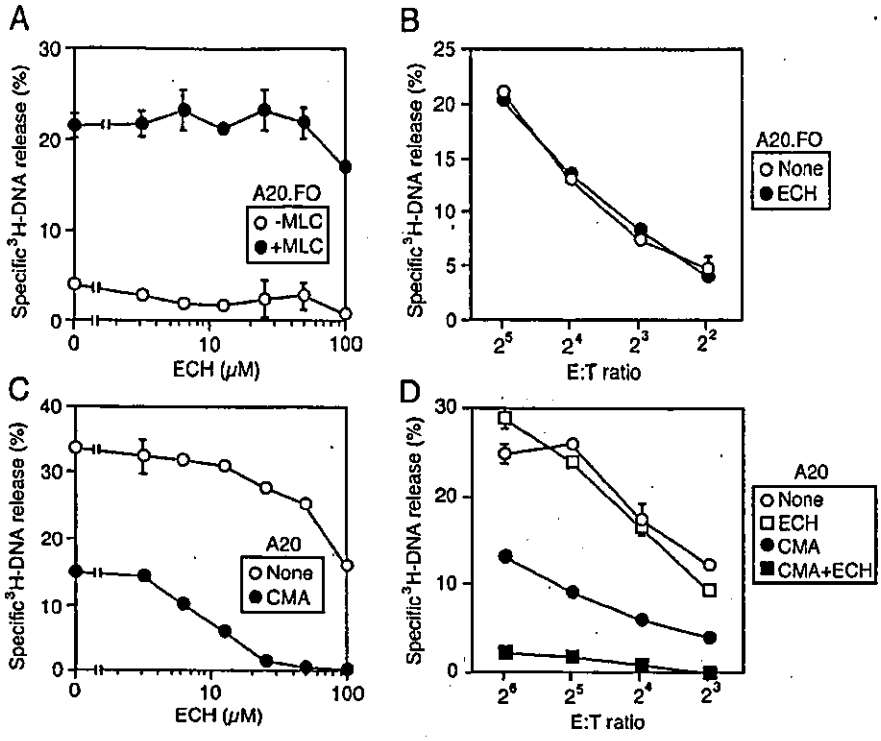

FIGURE 7. ECH selectively blocks FasL-based DNA fragmentation mediated by MLC cells. Responder spleen cells prepared from C57BL/6 mice were cultured with mitomycin C-treated stimulator spleen cells prepared from BALB/c mice for 4 days. *A*, [^{3}H]TdR-labeled A20.FO cells were pretreated with serial dilutions of ECH for 1 h. The target cells were mixed with (●) or without (○) MLC cells (E:T cell ratio = 32), then incubated for 4 h. *B*, [^{3}H]TdR-labeled A20.FO cells were pretreated with (●) or without (○) 50 μM ECH for 1 h. The target cells were mixed with different numbers of MLC cells, then incubated for 4 h. *C*, MLC cells were pretreated with (●) or without (○) 100 nM CMA for 2 h. [^{3}H]TdR-labeled A20 cells were pretreated with serial dilutions of ECH for 1 h. The target cells were mixed with MLC cells (E:T cell ratio = 16), then incubated for 4 h. *D*, MLC cells were pretreated with (● and ■) or without (○ and ●) 100 nM CMA for 2 h. [^{3}H]TdR-labeled A20 cells were pretreated with (■ and □) or without (● and ○) 50 μM ECH for 1 h. The target cells were mixed with different numbers of MLC cells, then incubated for 4 h. The radioactivity of fragmented DNA was measured. Data points represent the mean ± SD of triplicate cultures.

characterized by ssDNA nicks, which are mediated by granzyme A-activated DNase, NM23-H1 (34), whereas granzyme B initiates procaspase-3 processing, and the release of proapoptotic mitochondrial factors that facilitate the full activation of procaspase-3 (8–10). In the short term killing of target cells, granzyme B is critically involved in a rapid induction of DNA fragmentation (13). Consistent with this idea, the synthetic caspase inhibitor benzyloxycarbonyl-Val-Ala-Asp(OMe)-fluoromethyl ketone completely prevented DNA fragmentation of A20 cells induced by the CD8$^+$ CTL clone in the short term assay (data not shown), confirming that granzyme B is a main factor that induces DNA fragmentation in the perforin-dependent killing pathway. ECH failed to prevent the perforin/granzyme B-dependent DNA fragmentation. These findings provide additional evidence that ECH specifically inhibits death receptor-mediated apoptosis, but does not affect death receptor-independent apoptosis.

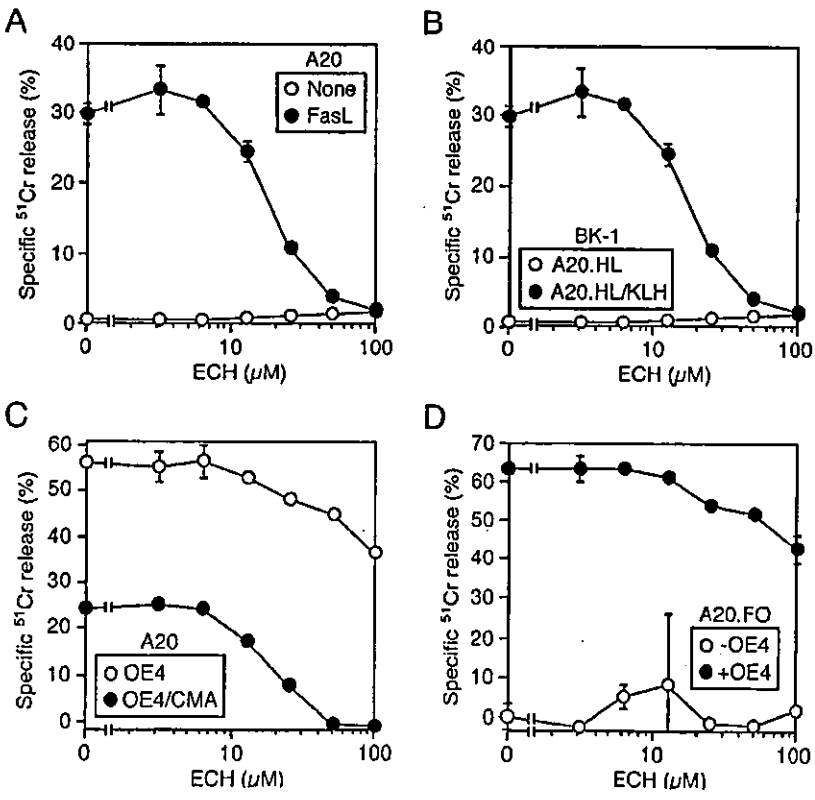

FIGURE 8. ECH inhibits FasL-dependent target cell lysis, but not perforin-dependent target cell lysis, in CTL-mediated cytotoxicity. *A*, ^{51}Cr-labeled A20 cells were preincubated with serial dilutions of ECH for 1 h, then incubated with (●) or without (○) cross-linked FasL (50 ng/ml) for 4 h. *B*, ^{51}Cr-labeled A20.HL cells were pulsed with or without KLH (300 μg/ml) before assay. KLH-pulsed A20.HL (●) and nonpulsed A20.HL (○) cells were preincubated with serial dilutions of ECH for 1 h. The target cells were mixed with BK-1 cells (E:T cell ratio = 8), then incubated for 4 h. *C*, OE4 cells were pretreated with (●) or without (○) 100 nM CMA for 2 h. ^{51}Cr-labeled A20 cells were pretreated with serial dilutions of ECH for 1 h. The target cells were mixed with OE4 cells (E:T cell ratio = 2), then incubated for 4 h. *D*, ^{51}Cr-labeled A20.FO cells were pretreated with serial dilutions of ECH for 1 h. The target cells were mixed with (●) or without (○) OE4 cells (E:T cell ratio = 2), then incubated for 4 h. The radioactivity of the supernatant was measured. Data points represent the mean ± SD of triplicate cultures.

The major molecular target of ECH in Fas-mediated apoptosis is procaspase-8, and ECH affected neither active caspase-8 nor activation of procaspase-3 and procaspase-9 at the cellular level (24). ECH has a molecular structure of α,β-unsaturated ketone and epoxide that might be reactive to thiol residues of proteins. In agreement with this hypothesis, glutathione or cysteine neutralized ECH binding to procaspase-8 (24). Recently, we have reported that the mycotoxin penicillic acid (PCA) inhibits Fas-mediated apoptosis by blocking activation of procaspase-8 (23). Although ECH and PCA are structurally unrelated, PCA exhibited the inhibitory activity similarly to ECH, in that PCA preferentially inhibited activation of procaspase-8, but did not affect active caspase-8 in living cells (23). Moreover, activation of procaspase-3 and procaspase-9 in the cell was only weakly inhibited by PCA (23). PCA contains α,β-unsaturated lactone able to bind to sulfhydryl groups. Analysis by mass spectrometry revealed that PCA binds to the cysteine residue of the active center in procaspase-8 (23). Although we have not yet determined the binding sites of ECH on procaspase-8, it seems likely that ECH binds to the active center cysteine and inactivates its intrinsic proteolytic activity.

DNA fragmentation was partially reversed when ECH was removed from A20 cells during the 4-h coculture with FasL. In our earlier paper (24), we showed that ECH affects neither cell surface Fas expression nor Fas-FasL interaction. Thus, it seems likely that a portion of procaspase-8 becomes functional by dissociation from ECH or is newly synthesized during the 4-h incubation, although we cannot rule out the possibility that ECH affects FasL expression on CTL.

In the short term culture, ECH alone did not induce apoptosis or necrosis. However, in the long term culture, ECH markedly reduced live cells without an induction of DNA fragmentation, whereas a portion of ECH-treated cells became positive for trypan blue staining. Thus, these results indicate that ECH inhibits proliferation, but can also induce necrotic cell death in the long term culture. Molecular mechanisms of ECH on inhibiting proliferation or inducing necrosis remain to be elucidated.

ECH inhibited Fas-mediated apoptosis in several human cell lines (24) (data not shown) and two murine lymphoma cell lines tested in this paper at the minimum inhibitory concentrations of ECH ranging from 10–100 μM. ECH inhibited Fas-mediated apoptosis at relatively lower concentrations in human cell lines (24), and 100 μM ECH was required for the complete inhibition of the Fas-mediated apoptosis in L5178Y-Fas cells. The culture medium for murine lymphoma cells contains 50 μM 2-ME, which might neutralize ECH due to the presence of thiol residues. However, the inhibitory doses of ECH unaltered in culture medium without 2-ME (data not shown). In addition, the FasL susceptibility is unlikely to involve the inhibitory doses of ECH, because L5178Y-Fas cells and A20 cells were equivalently susceptible to FasL, but Fas-mediated apoptosis in A20 cells was more strongly inhibited by ECH. A possible explanation might be that intracellular competitors such as glutathione and/or thiol-containing protein(s) antagonize ECH and determine the strength of its inhibitory activity on procaspase-8.

We previously showed that CMA is a specific inhibitor of the perforin-dependent killing pathway (18). CMA induces inactivation and subsequent proteolytic degradation of perforin in lytic granules upon neutralization of acidic pH (17, 19, 20). By contrast, the FasL-dependent killing pathway mediated by Ag-specific CTL was suppressed by an inhibitor of glycoprotein transport, brefeldin A (18), as FasL is newly synthesized upon TCR activation and transported to the cell surface. Ca^{2+} dependency was frequently used to distinguish between the perforin-based cytotoxicity and the FasL-based cytotoxicity. However, Ca^{2+} is not only required for the function of perforin, but also for TCR-mediated early signaling leading to FasL expression (35–37). Therefore, the Ca^{2+}-independent cytotoxicity previously observed is largely due to the preexisting FasL and is believed to be insensitive to brefeldin A. As ECH blocks activation of procaspase-8 in target cells, it is thought that ECH is a more general nonpeptide inhibitor of the FasL-mediated killing pathway exerted by CTL, NK cells, or other types of cells, even though they constitutively express cell surface FasL.

The Fas/FasL system plays an essential role in lymphocyte homeostasis, and mutations in this system lead to the accumulation of abnormal T cells in the peripheral lymphoid organs and the development of severe autoimmune diseases in humans and mice (3–5). In addition to death-inducing functions, our and other groups reported that Fas provides costimulatory signals for human T cells, and caspase inhibitors block T cell proliferation (38–40), suggesting that caspase activation is required for T cell proliferation. The FasL-dependent killing of target cells by CTL is involved in the pathogenesis of experimental autoimmune encephalomyelitis and fulminant hepatitis (41–43). In neuronal diseases such as Huntington diseases, procaspase-8 is activated independently of death receptors (44, 45). Taken together, caspase-8 inhibitors such as ECH might be therapeutic candidates to treat autoimmune diseases and neuronal diseases.

Mice deficient in perforin, granzymes, Fas, or FasL have been used to study the biological significance of the perforin/granzyme system and the Fas/FasL system in various in vivo models and in vitro killing assays. These knockout mice, however, are not always applicable to all experimental settings. In this report we have shown that ECH is a specific inhibitor of the FasL-dependent killing pathway, but does not affect the perforin/granzyme-dependent killing pathway. Thus, ECH is a highly useful tool to evaluate the FasL-dependent killing pathway in cell-mediated cytotoxicity and might be applicable for all CTL-target combinations.

Acknowledgments

We thank Dr. N. Shinohara for CTL clones and their target cells, and Drs. J. Tschopp and H. Yagita for reagents. We also thank Dr. R. C. Budd for critical reading of the manuscript.

References

1. Russell, J. H., and T. J. Ley. 2002. Lymphocyte-mediated cytotoxicity. *Annu. Rev. Immunol. 20:323.*
2. Barry, M., and R. C. Bleackley. 2002. Cytotoxic T lymphocytes: all roads lead to death. *Nat. Rev. Immunol. 2:401.*
3. Nagata, S. 1997. Apoptosis by death factor. *Cell 88:355.*
4. Krammer, P. H. 2000. CD95's deadly mission in the immune system. *Nature 407:789.*
5. Siegel, R. M., F. K.-M. Chan, H. J. Chun, and M. J. Lenardo. 2000. The multifaceted role of Fas signaling in immune cell homeostasis and autoimmunity. *Nat. Immunol. 1:469.*
6. Griffiths, G. M., and Y. Argon. 1995. Structure and biogenesis of lytic granules. *Curr. Top. Microbiol. Immunol. 198:39.*
7. Metkar, S. S., B. Wang, M. Aguilar-Santelises, S. M. Raja, L. Uhlin-Hansen, E. Podack, J. A. Trapani, and C. J. Froelich. 2002. Cytotoxic cell granule-mediated apoptosis: perforin delivers granzyme B-serglycin complexes into target cells without plasma membrane pore formation. *Immunity 16:417.*
8. Sutton, V. R., M. E. Wowk, M. Cancilla, and J. A. Trapani. 2003. Caspase activation by granzyme B is indirect, and caspase autoprocessing requires the release of proapoptotic mitochondrial factors. *Immunity 18:319.*
9. Goping, I. S., M. Barry, P. Liston, T. Sawchuk, G. Constantinescu, K. M. Michalak, I. Shostak, D. L. Roberts, A. M. Hunter, R. Korneluk, et al. 2003. Granzyme B-induced apoptosis requires both direct caspase activation and relief of caspase inhibition. *Immunity 18:355.*
10. Metkar, S. S., B. Wang, M. L. Ebbs, J. H. Kim, Y. J. Lee, S. M. Raja, and C. J. Froelich. 2003. Granzyme B activates procaspase-3 which signals a mitochondrial amplification loop for maximal apoptosis. *J. Cell Biol. 160:875.*
11. Beresford, P. J., Z. Xia, A. H. Greenberg, and J. Lieberman. 1999. Granzyme A loading induces rapid cytolysis and a novel form of DNA damage independently of caspase activation. *Immunity 10:585.*
12. Shresta, S., T. A. Graubert, D. A. Thomas, S. Z. Raptis, and T. J. Ley. 1999. Granzyme A initiates an alternative pathway for granule-mediated apoptosis. *Immunity 10:595.*

13. Heusel, J. W., R. L. Wesselschmidt, S. Shresta, J. H. Russell, and T. J. Ley. 1994. Cytotoxic lymphocytes require granzyme B for the rapid induction of DNA fragmentation and apoptosis in allogeneic target cells. *Cell 76:977.*
14. Kischkel, F. C., S. Hellbardt, I. Behrmann, M. Germer, M. Pawlita, P. H. Krammer, and M. E. Peter. 1995. Cytotoxicity-dependent APO-1 (Fas/CD95)-associated proteins form a death-inducing signaling complex (DISC) with the receptor. *EMBO J. 14:5579.*
15. Boatright, K. M., M. Renatus, F. L. Scott, S. Sperandio, H. Shin, I. M. Pedersen, J.-E. Ricci, W. A. Edris, D. P. Sutherlin, D. R. Green, et al. 2003. A unified model for apical caspase activation. *Mol. Cell 11:529.*
16. Donepudi, M., A. M. Sweeney, C. Briand, and M. G. Grütter. 2003. Insights into the regulatory mechanism for caspase-8 activation. *Mol. Cell 11:543.*
17. Kataoka, T., K. Takaku, J. Magae, N. Shinohara, H. Takayama, S. Kondo, and K. Nagai. 1994. Acidification is essential for maintaining the structure and function of lytic granules of CTL. *J. Immunol. 153:3938.*
18. Kataoka, T., N. Shinohara, H. Takayama, K. Takaku, S. Kondo, S. Yonehara, and K. Nagai. 1996. Concanamycin A, a powerful tool for characterization and estimation of contribution of perforin- and Fas-based lytic pathways in cell-mediated cytotoxicity. *J. Immunol. 156:3678.*
19. Kataoka, T., M. Sato, S. Kondo, and K. Nagai. 1996. Estimation of pH and the number of lytic granules in a $CD8^+$ CTL clone treated with an inhibitor of vacuolar type H^+-ATPase, concanamycin A. *Biosci. Biotech. Biochem. 60:1729.*
20. Kataoka, T., K. Togashi, H. Takayama, K. Takaku, and K. Nagai. 1997. Inactivation and proteolytic degradation of perforin within lytic granules upon neutralization of acidic pH. *Immunology 91:493.*
21. Bando, M., Y. Miyake, M. Shiina, M. Wachi, K. Nagai, and T. Kataoka. 2002. Actin cytoskeleton is required for early apoptosis signaling induced by anti-Fas antibody but not Fas ligand in murine B lymphoma A20 cells. *Biochem. Biophys. Res. Commun. 290:268.*
22. Kataoka, T., M. Ito, R. C. Budd, J. Tschopp, and K. Nagai. 2002. Expression level of c-FLIP versus Fas determines susceptibility to Fas ligand-induced cell death in murine thymoma EL-4 cells. *Exp. Cell Res. 273:256.*
23. Bando, M., M. Hasegawa, Y. Tsuboi, Y. Miyake, M. Shiina, M. Ito, H. Handa, K. Nagai, and T. Kataoka. 2003. The mycotoxin penicillic acid inhibits Fas ligand-induced apoptosis by blocking self-processing of caspase-8 in death-inducing signaling complex. *J. Biol. Chem. 278:5786.*
24. Miyake, Y., H. Kakeya, T. Kataoka, and H. Osada. 2003. Epoxycyclohexenone inhibits Fas-mediated apoptosis by blocking activation of pro-caspase-8 in the death-inducing signaling complex. *J. Biol. Chem. 278:11213.*
25. Kanbayashi, K., T. Kamikakiuchi, and I. Horibe. 1999. Japan Kokai Patent H11-222456.
26. Staerz, U. D., O. Kanagawa, and M. J. Bevan. 1985. Hybrid antibodies can target sites for attack by T cells. *Nature 314:628.*
27. Shinohara, N., Y.-Y. Huang, and A. Muroyama. 1991. Specific suppression of antibody responses by soluble protein-specific, class II-restricted cytolytic T lymphocyte clones. *Eur. J. Immunol. 21:23.*
28. Watanabe, M., D. R. Wegmann, A. Ochi, and N. Hozumi. 1986. Antigen presentation by a B-cell line transfected with cloned immunoglobulin heavy- and light-chain genes specific for a defined hapten. *Proc. Natl. Acad. Sci. USA 83:5247.*
29. Hanabuchi, S., M. Koyanagi, A. Kawasaki, N. Shinohara, A. Matsuzawa, Y. Nishimura, Y. Kobayashi, S. Yonehara, H. Yagita, and K. Okumura. 1994. Fas and its ligand in a general mechanism of T-cell-mediated cytotoxicity. *Proc. Natl. Acad. Sci. USA 91:4930.*
30. Schneider, P., N. Holler, J.-L. Bodmer, M. Hahne, K. Frei, A. Fontana, and J. Tschopp. 1998. Conversion of membrane-bound Fas(CD95) ligand to its soluble form is associated with downregulation of its proapoptotic activity and loss of liver toxicity. *J. Exp. Med. 187:1205.*
31. Luce, G. G., S. O. Sharrow, S. Shaw, and P. M. Gallop. 1985. Enumeration of cytotoxic cell-target cell conjugates by flow cytometry using internal fluorescent stains. *BioTechniques 3:270.*
32. Kawasaki, A., Y. Shinkai, Y. Kuwana, A. Furuya, Y. Iigo, N. Hanai, S. Itoh, H. Yagita, and K. Okumura. 1990. Perforin, a pore-forming protein detectable by monoclonal antibodies, is a functional marker for killer cells. *Int. Immunol. 2:677.*
33. Takayama, H., N. Shinohara, A. Kawasaki, Y. Someya, S. Hanaoka, H. Kojima, H. Yagita, K. Okumura, and Y. Shinkai. 1991. Antigen-specific directional target cell lysis by perforin-negative T lymphocyte clones. *Int. Immunol. 3:1149.*
34. Fan, Z., P. J. Beresford, D. Y. Oh, D. Zhang, and J. Lieberman. 2003. Tumor suppressor NM23–H1 is a granzyme A-activated DNase during CTL-mediated apoptosis, and the nucleosome assembly protein SET is its inhibitor. *Cell 112:659.*
35. Kojima, H., N. Shinohara, S. Hanaoka, Y. Someya-Shirota, Y. Takagaki, H. Ohno, T. Saito, T. Katayama, H. Yagita, K. Okumura, et al. 1994. Two distinct pathways of specific killing revealed by perforin mutant cytotoxic T lymphocytes. *Immunity 1:357.*
36. Garner, R., C. D. Helgason, E. A. Atkinson, M. J. Pinkoski, H. L. Ostergaard, O. Sorensen, A. Fu, P. H. Lapchak, A. Rabinovitch, J. E. McElhaney, et al. 1994. Characterization of a granule-independent lytic mechanism used by CTL hybridomas. *J. Immunol. 153:5413.*
37. Vignaux, F., E. Vivier, B. Malissen, V. Depraetere, S. Nagata, and P. Golstein. 1995. TCR/CD3 coupling to Fas-based cytotoxicity. *J. Exp. Med. 181:781.*
38. Alderson, M. R., R. J. Armitage, E. Maraskovsky, T. W. Tough, E. Roux, K. Schooley, F. Ramsdell, and D. H. Lynch. 1993. Fas transduces activation signals in normal human T lymphocytes. *J. Exp. Med. 178:2231.*
39. Alam, A., L. Y. Cohen, S. Aouad, and R.-P. Sékaly. 1999. Early activation of caspases during T lymphocyte stimulation results in selective substrate cleavage in nonapoptotic cells. *J. Exp. Med. 190:1879.*
40. Kennedy, N. J., T. Kataoka, J. Tschopp, and R. C. Budd. 1999. Caspase activation is required for T cell proliferation. *J. Exp. Med. 190:1891.*
41. Okuda, Y., C. C. Bernard, H. Fujimura, T. Yanagihara, and S. Sakoda. 1998. Fas has a crucial role in the progression of experimental autoimmune encephalomyelitis. *Mol. Immunol. 35:317.*
42. Dittel, B. N., R. M. Merchant, and C. A. Janeway, Jr. 1999. Evidence for Fas-dependent and Fas-independent mechanisms in the pathogenesis of experimental autoimmune encephalomyelitis. *J. Immunol. 162:6392.*
43. Kondo, T., T. Suda, H. Fukuyama, M. Adachi, and S. Nagata. 1997. Essential roles of the Fas ligand in the development of hepatitis. *Nat. Med. 3:409.*
44. Sanchez, I., C. J. Xu, P. Juo, A. Kakizaka, J. Blenis, and J. Yuan. 1999. Caspase-8 is required for cell death induced by expanded polyglutamine repeats. *Neuron 22:623.*
45. Gervais, F. G., R. Singaraja, S. Xanthoudakis, C.-A. Gutekunst, B. R. Leavitt, M. Metzler, A. S. Hackam, J. Tam, J. P. Vaillancourt, V. Houtzager, et al. 2002. Recruitment and activation of caspase-8 by the Huntingtin-interacting protein Hip-1 and a novel partner Hippi. *Nat. Cell Biol. 4:95.*

JOC Article

Different Reaction Modes for the Oxidative Dimerization of Epoxyquinols and Epoxyquinones. Importance of Intermolecular Hydrogen-Bonding

Mitsuru Shoji,[†] Hiroki Imai,[†] Isamu Shiina,[‡] Hideaki Kakeya,[§] Hiroyuki Osada,[§] and Yujiro Hayashi*,[†]

Department of Industrial Chemistry, Faculty of Engineering, and Department of Applied Chemistry, Faculty of Science, Tokyo University of Science, Kagurazaka, Shinjuku-ku, Tokyo 162-8601, and Antibiotics Laboratory, Discovery Research Institute, RIKEN, 2-1 Hirosawa, Wako, Saitama 351-0198, Japan

hayashi@ci.kagu.tus.ac.jp

Received October 16, 2003

An oxidative dimerization reaction, involving the three successive steps of oxidation, 6π-electrocyclization, and Diels–Alder reaction, has been experimentally and theoretically investigated for the three 2-alkenyl-3-hydroxymethyl-2-cyclohexen-1-one derivatives epoxyquinol **3**, epoxyquinone **6**, and cyclohexenone **10**. Of the sixteen possible modes of the oxidation/6π-electrocylization/Diels–Alder reaction cascade for the epoxyquinone **6**, and eight for the cyclohexenone **10**, only the *endo-anti*(epoxide)-*anti*(Me)-hetero and *endo-anti*(Me)-hetero modes are, respectively, observed, while both *endo-anti*(epoxide)-*anti*(Me)-hetero and *exo-anti*(epoxide)-*anti*(Me)-homo reaction modes occur with the epoxyquinol **3**. Intermolecular hydrogen-bonding is found to be the key cause of formation of both epoxyquinols A and B with **3**, although epoxyquinone **6** and cyclohexenone **10** both gave selectively only the epoxyquinol A-type product. In the dimerization of epoxyquinol **3**, two monomer 2*H*-pyrans **5** interact with each other to afford intermediate complex **28** or **29** stabilized by hydrogen-bonding, from which Diels–Alder reaction proceeds. Theoretical calculations have also revealed the differences in the reaction profiles of epoxyquinone **6** and cyclohexenone **10**. Namely, the rate-determining step of the former is the Diels–Alder reaction, while that of the latter is the 6π-electrocyclization.

We have recently isolated and determined the structures of epoxyquinols A (**1**)[1] and B (**2**),[2] which are novel angiogenesis inhibitors with a highly functionalized and complicated heptacyclic ring system containing 12 stereocenters. Although these structures are very complex, we have proposed that they arise biosynthetically from the rather simple epoxyquinol **3** via an oxidation/6π-electrocyclization/Diels–Alder reaction cascade (Scheme 1). Recently we have accomplished the first asymmetric total synthesis of these molecules and determined their absolute stereochemistry.[3] Key steps of this synthesis are the $HfCl_4$-mediated Diels–Alder reaction of furan with the acrylate of Corey's chiral auxiliary[4] and a biomimetic, oxidative Diels–Alder reaction of monomer **3**. We have also established a practical synthetic route to both

SCHEME 1. Key Steps for the Synthesis of Epoxyquinols A and B

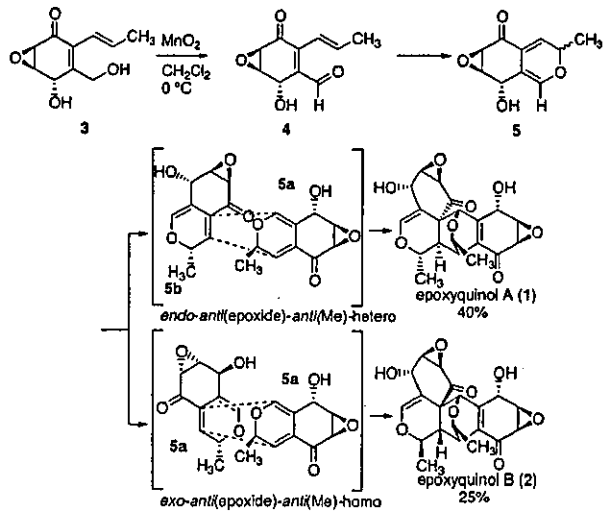

enantiomers of epoxyquinols A and B using the chromatography-free preparation of an iodolactone and a lipase-mediated kinetic resolution as key steps.[5] Soon after our first synthesis, Porco et al. published a synthesis of

* To whom correspondence should be addressed. Phone: (+81)3-5228-8318. Fax: (+81)3-5261-4631.
† Department of Industrial Chemistry, Faculty of Engineering.
‡ Department of Applied Chemistry, Faculty of Science.
§ RIKEN.

(1) Kakeya, H.; Onose, R.; Koshino, H.; Yoshida, A.; Kobayashi, K.; Kageyama, S.-I.; Osada, H. *J. Am. Chem. Soc.* **2002**, *124*, 3496.
(2) Kakeya, H.; Onose, R.; Yoshida, A.; Koshino, H.; Osada, H. *J. Antibiot.* **2002**, *55*, 829.
(3) Shoji, M.; Yamaguchi, J.; Kakeya, H.; Osada, H.; Hayashi, Y. *Angew. Chem., Int. Ed.* **2002**, *41*, 3192.
(4) (a) Hayashi, Y.; Nakamura, M.; Nakao, S.; Inoue, T.; Shoji, M. *Angew. Chem., Int. Ed.* **2002**, *41*, 4079. (b) Sarakinos, G.; Corey, E. J. *Org. Lett.* **1999**, *1*, 1741.

10.1021/jo0355303 CCC: $27.50
Published on Web 01/27/2004

SCHEME 2. **Oxidative Dimerization of Hydroxyepoxyquinone 3 with DMP**

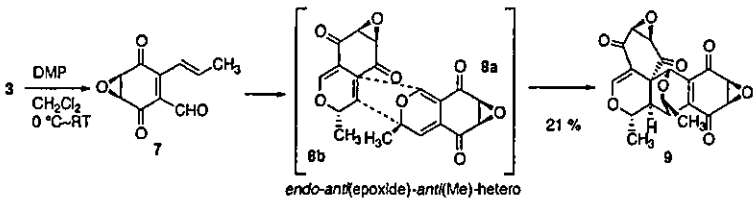

epoxyquinols A and B,[6] and just recently Mehta et al. have also reported the synthesis of racemic epoxyquinols A and B.[7]

While epoxyquinols A and B are epoxyquinol dimers, torreyanic acid, isolated from an endophytic fungus, *Pestalotiopsis microspra*, is an epoxyquinone dimer.[8] The proposed biosynthesis of torreyanic acid also involves an oxidation/6π-electrocyclization/Diels–Alder reaction cascade, and Porco et al. have developed an elegant biomimetic total synthesis, backed up by theoretical calculations, in which only the epoxyquinol A-type dimer is selectively formed.[9]

In the course of our total synthesis of epoxyquinols A and B, we examined carefully the oxidation of monomer **3** and observed the following interesting phenomenon: When monomer **3** was treated with the Dess–Martin periodinane (DMP),[10] both primary and secondary hydroxy groups were oxidized, affording cyclized 2*H*-pyran derivatives **8a/b**, which gave epoxyquinol A-type product **9** in 21% yield without formation of the epoxyquinol-B type product (Scheme 2). The yield of **9** was increased to 70% when isolated epoxyquinone **6** was treated with DMP (vide infra, Scheme 6).

The reaction modes for the Diels–Alder reaction initiated by oxidation of epoxyquinol **3** can be classified as follows: Consider the diene part first. The reacting face of the diene is either *anti* or *syn* to the epoxide and *anti* or *syn* to the methyl group, which we designate as *anti*(epoxide) or *syn*(epoxide) and *anti*(Me) or *syn*(Me) additions, respectively. When the diene and dienophile molecules are the same, we call it homocoupling, while heterocoupling is the reaction in which the diene and dienophile components are different. *Endo* addition is an addition in which the secondary orbital interaction between the carbonyl of the dienophile and the diene is present, while *exo* addition is an addition without such an interaction. According to this classification, epoxyquinols A and B are dimers of *endo-anti*(epoxide)-*anti*(Me)-hetero addition and *exo-anti*(epoxide)-*anti*(Me)-homo addition, respectively. In the dimerization of epoxyquinol **3**, the only two reaction modes observed are the *endo-anti*(epoxide)-*anti*(Me)-hetero and *exo-anti*(epoxide)-*anti*(Me)-homo modes, while the dimerization of epoxyquinone **6** proceeds via a single mode, the *endo-anti*(epoxide)-*anti*(Me)-hetero mode.

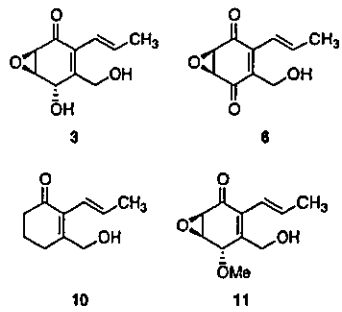

FIGURE 1. Monomers **3**, **6**, **10**, and **11**.

To understand the difference in reaction modes between epoxyquinol **3** and epoxyquinone **6**, the oxidative dimerization of a parent monomer, **10**, without epoxide and hydroxy groups, has been examined. The methoxycyclohexenone **11** was also investigated to shed light on the effect of the hydroxy group in **3**. In this paper we describe our investigation of the oxidation/6π-electrocyclization/Diels–Alder reaction by systematic comparison using the four monomers **3**, **6**, **10**, and **11** together with theoretical calculations (Figure 1).[11]

Results and Discussion

Synthesis of Monomers. Synthesis of the epoxyquinol monomer **3** has already been described.[3,5] The epoxyquinone monomer **6** was prepared from epoxyquinol monomer **3** according to Scheme 3, by protection of the primary alcohol with TBS, followed by oxidation with DMP and deprotection. The methoxy monomer **11** was prepared from **12** by methyl ether formation[12] and deprotection of the TBS group as shown in Scheme 4. The cyclohexenone monomer **10** with neither epoxy nor hydroxy functionalities was prepared according to Scheme 5. 3-Ethoxy-2-cyclohexene-1-one (**15**)[13] was treated with $LiCH_2SPh$[14] to afford 3-(phenylthiomethyl)-2-cyclohexen-1-one (**16**), which was converted to 3-formyl-2-cyclohexen-1-one (**18**) via Pummerer rearrangement.[15] Reduction with $CeCl_3$–$NaBH_4$,[16] protection of the primary hydroxy group, and

(5) Shoji, M.; Kishida, S.; Takeda, M.; Kakeya, H.; Osada, H.; Hayashi, Y. *Tetrahedron Lett.* **2002**, *43*, 9155.
(6) Li, C.; Bardhan, S.; Pace, E. A.; Liang, M.-C.; Gilmore, T. D.; Porco, J. A., Jr. *Org. Lett.* **2002**, *4*, 3267.
(7) Mehta, G.; Islam, K. *Tetrahedron Lett.* **2003**, *44*, 3569.
(8) (a) Lee, J. C.; Yang, X.; Schwartz, M.; Strobel, G. A.; Clardy, J. *Chem. Biol.* **1995**, *2*, 721. (b) Lee, J. C.; Strobel, G. A.; Lobkovsky, E.; Clardy, J. *J. Org. Chem.* **1996**, *61*, 3232. (c) Jarvis, B. B. *Chemtracts* **1997**, *10*, 10.
(9) (a) Li, C.; Lobkovsky, E.; Porco, J. A., Jr. *J. Am. Chem. Soc.* **2000**, *122*, 10484. (b) Li, C.; Johnson, R. P.; Porco, J. A., Jr. *J. Am. Chem. Soc.* **2003**, *125*, 5095.
(10) (a) Dess, D. B.; Martin, J. C. *J. Org. Chem.* **1983**, *48*, 4155. (b) Dess, D. B.; Martin, J. C. *J. Am. Chem. Soc.* **1991**, *113*, 7277. (c) Ireland, R. E.; Liu, L. *J. Org. Chem.* **1993**, *58*, 2899.
(11) A preliminary communication of this work has been reported; see: Shoji, M.; Kishida, S.; Kodera, Y.; Shiina, I.; Kakeya, H.; Osada, H.; Hayashi, Y. *Tetrahedron Lett.* **2003**, *44*, 7205.
(12) Greene, A. E.; Drian, C. L.; Crabbe, P. *J. Am. Chem. Soc.* **1980**, *102*, 7583.
(13) Gannon, W. F.; House, H. O. *Organic Syntheses*; Wiley & Sons: New York, 1973; Collect. Vol. V, p 539.
(14) Corey, E. J.; Seebach, D. *J. Org. Chem.* **1966**, *31*, 4097.
(15) Ishibashi, H.; Kameoka, C.; Kodama, K.; Ikeda, M. *Tetrahedron* **1996**, *52*, 489.
(16) Gemal, A. L.; Luche, J.-L. *J. Am. Chem. Soc.* **1981**, *103*, 5454.